Progress In Electromagnetics Research, Vol. 149, 15–44, 2014

Surface and Volume Integral Equation Methods for Time-Harmonic Solutions of Maxwell's Equations

Pasi Ylä-Oijala[1, *], Johannes Markkanen[2], Seppo Järvenpää[1], and Sami P. Kiminki[1]

(*Invited Paper*)

Abstract—During the last two-three decades the importance of computer simulations based on numerical full-wave solutions of Maxwell's has continuously increased in electrical engineering. Software products based on integral equation methods have an unquestionable importance in the frequency domain electromagnetic analysis and design of open-region problems. This paper deals with the surface and volume integral equation methods for finding time-harmonic solutions of Maxwell's equations. First a review of classical integral equation representations and formulations is given. Thereafter we briefly overview the mathematical background of integral operators and equations and their discretization with the method of moments. The main focus is on advanced techniques that would enable accurate, stable, and scalable solutions on a wide range of material parameters, frequencies and applications. Finally, future perspectives of the integral equation methods for solving Maxwell's equations are discussed.

1. INTRODUCTION

Our modern world of wireless communications, portable electronics, microwave and other electrical devices and instruments is built upon fundamental theory of electromagnetics (EM) [1, 2]. This theory is summarized by Maxwell's equations [3, 4] — the partial differential equations of EM. Maxwell's equations have been proven to be valid for very different length scales, from subatomic to intergalactic length scales [5], and they also have a highly predictive power. Once solutions to Maxwell's equations are found, they often can predict the experimental outcome reliably and accurately [6]. The ability to perform numerical simulations based on full-wave solutions of Maxwell's equations has therefore become increasingly important for research and development in various fields of modern electrical engineering.

Maxwell's equations lead to complicated mathematical and numerical models that are challenging to solve. Analytical solutions are available only in very rare simplified cases, and complex three-dimensional (3D) real-world engineering problems call for more general numerical approaches. This gives rise to Computational Electromagnetics (CEM), a branch of computational science and engineering that especially focuses on numerical modeling and simulations of EM phenomena. CEM finds applications from nano-scale plasmonics and artificial material (metamaterial) structures to photonics, from wireless sensors and communication devices to Earth observations and remote sensing, and from biomedical and bioimaging instruments to radars and antenna arrays. This large variety of applications, materials, geometries and frequency ranges leads to a very rich domain of theoretical and computational aspects, making CEM fascinating and interdisciplinary realm of science arising from Maxwell's equations.

Full-wave methods in CEM can be generally classified as partial differential equation methods (PDEMs) and as integral equation methods (IEMs). The difference here is that PDEMs, such as

Received 1 July 2014, Accepted 21 August 2014, Scheduled 23 August 2014
Invited paper for the Commemorative Collection on the 150-Year Anniversary of Maxwell's Equations.
* Corresponding author: Pasi Ylä-Oijala (pasi.yla-oijala@aalto.fi).
[1] Department of Radio Science and Engineering, Aalto University, Finland. [2] Department of Physics, University of Helsinki, Finland.

the finite element method (FEM) [7–9], and the method of finite differences (FD) [10–12], typically consider directly solutions of Maxwell's equations, whereas in the IEMs the problem of solving Maxwell's equations is reformulated as integral equations for equivalent sources [5, 13, 14]. IEMs provide elegant solutions for many open-region scattering and radiation problems in particular to those formulated with mathematical boundary conditions. These boundary conditions allows one to restrict the equations and sources to the boundary of an object. This leads to the surface integral equation (SIE) method; the method that reduces the dimensionality of the problem by one, and therefore allows significant reduction on the number of degrees of freedom (dof), as well as much simplified geometry and data representations. In cases where the SIE methods are not available, integral equations based on volume discretizations [15], i.e., volume integral equation methods (VIEs), are required.

An IEM starts by formulating the problem in terms of integral equations and equivalent sources. Then a discretization strategy is applied to approximate the unknown functions and to convert the continuous equations into discrete ones. Finally, the resulting finite system of linear equations (matrix equation) is solved. To develop efficient and stable numerical EM simulation software based on integral equations is, however, far from being a trivial task. Integral equations and their numerical discretization and implementation are plagued with several theoretical and practical challenges and obstacles, such as low frequency instabilities and dense-mesh breakdown. In addition, the matrix equations arising from discretization of integral equations are fully-populated and expensive to solve.

This paper deals with the surface and volume IEMs for finding time-harmonic solutions of Maxwell's equations. First we review the classical integral equation representations and formulations. Thereafter, brief overviews of the mathematical background of the integral operators and equations, and their discretization with the method of moments are given. The main focus is on advanced techniques — formulations, discretization strategies, regularization, and fast solvers — that would lead to an algorithm with the following properties:

(i) *Accuracy*: The results should be accurate and converge towards the correct solution as the number of dof is increased.

(ii) *Stability*: The solution should be stable. Small changes on the initial conditions should only result in small changes on the solution.

(iii) *Scalability*: The amount of required computer resources should not increase too much as the size of the problem is enlarged.

Finally, some future perspectives of the EM IEMs are discussed.

2. HISTORICAL OVERVIEW

The IEMs for solving Maxwell's equations have been around for a long time [16]. The advent of computers in the 60' opened new possibilities for numerical methods. First numerical solutions of integral equations were developed for simplified two-dimensional (2D) problems, such as scattering by infinitely long cylinders [17–19]. The first class of three-dimensional (3D) problems consisted wire antennas and scatterers [20, 21]. In the turn of 70's and 80's methods were developed for (3D) rotationally symmetric structures — "bodies of revolution" [22–24]. A significant step towards solution of 3D problems involving arbitrary geometries was presented in 1982 [25]. In that celebrated paper, a basis function, nowadays known as the Rao-Wilton-Glisson (RWG) function, was introduced and used to expand surface current densities on planar arbitrarily shaped surface patches (triangles).

The discovery of the RWG basis functions made it possible to develop more general numerical methods and to solve complex scattering and radiation problems involving arbitrarily shaped 3D dielectric [26], composite metallic and dielectric [27], as well as impedance bodies [28]. However, soon the high computational complexity of the IEMs became a major bottleneck in the practical simulations, and so it was crucial to come up with techniques that would reduce the high computational load of the IEMs and enable efficient solutions of large-scale problems. These techniques, known as *fast integral equation solvers*, significantly extended the usability of the IEMs and made IEMs very compatible with the computationally less expensive PDEMs [6, 29].

The first fast integral equation solvers for 3D structures were based on the CG-FFT (Conjugate Gradient-Fast Fourier Transform) method [30–33]. These methods effectively reduced the high

computational load of the IEMs, but required uniform rectangular grid and thus had rather limited capacity of modeling arbitrarily shaped structures. More versatile methods, like the adaptive integral method (AIM) [34] and the precorrected FFT method (pFFT) [35], were developed in the 90's. Another approach, also available for arbitrary meshes and geometries, is the fast multipole method (FMM) [36]. The multilevel version of FMM, multilevel fast multipole algorithm (MLFMA), introduced in the mid 90's [37–39], have had a significant impact on the solution of large-scale problems with the IEMs. Recent parallel implementations of MLFMA are able to solve problems with the order 10^8 dof [40, 41].

The fast integral equation solvers, as effective they are, may not alone be sufficient, and the poor convergence of an iterative solution is a bottleneck. It became extremely important to develop techniques that would improve conditioning of the linear system. In the 21st century research on various regularization and preconditioning techniques [42–47] as well as on novel integral equation formulations [48–52] and discretization techniques [53–60] has been very active. The research on these areas is still ongoing [61].

3. BACKGROUND

This section provides background for the rest of the paper. We introduce EM theory needed to formulate integral equations for time-harmonic solutions of Maxwell's equations, and briefly review mathematical background of the integral operators and equations and their discretization with MoM.

3.1. Maxwell's Equations and Boundary Conditions

Maxwell's equations are the fundamental partial differential equations of EM. These equations, supplemented with constitute relations of matter, boundary, and interface conditions, describe interaction of EM waves with material. For time-harmonic fields, with time convention $e^{-i\omega t}$, Maxwell's equations in a linear and source free domain read

$$\nabla \times \mathbf{E} = i\omega \mathbf{B}, \tag{1}$$

$$\nabla \times \mathbf{H} = -i\omega \mathbf{D}, \tag{2}$$

$$\nabla \cdot \mathbf{D} = 0, \tag{3}$$

$$\nabla \cdot \mathbf{B} = 0. \tag{4}$$

The field intensities $\mathbf{E}$ and $\mathbf{H}$ are related to the flux densities $\mathbf{D}$ and $\mathbf{B}$ via the constitutive relations

$$\mathbf{D} = \bar{\bar{\varepsilon}} \cdot \mathbf{E} \quad \text{and} \quad \mathbf{B} = \bar{\bar{\mu}} \cdot \mathbf{H}, \tag{5}$$

where $\bar{\bar{\varepsilon}}$ and $\bar{\bar{\mu}}$ are dyadic *electric permittivity* and *magnetic permeability*. A medium is called homogeneous if functions $\bar{\bar{\varepsilon}}$ and $\bar{\bar{\mu}}$ are constants, otherwise the medium is inhomogeneous. If $\bar{\bar{\varepsilon}}$ and $\bar{\bar{\mu}}$ are scalar, the medium is isotropic, otherwise it is anisotropic. Generalization of this is a bi-anisotropic medium with constitutive relations [62]

$$\mathbf{D} = \bar{\bar{\varepsilon}} \cdot \mathbf{E} + \bar{\bar{\xi}} \cdot \mathbf{H} \quad \text{and} \quad \mathbf{B} = \bar{\bar{\mu}} \cdot \mathbf{H} + \bar{\bar{\zeta}} \cdot \mathbf{E}, \tag{6}$$

where $\bar{\bar{\xi}}$ and $\bar{\bar{\zeta}}$ are the magneto-electric material parameters.

On interfaces between two media with different material properties the solutions of Maxwell's equations should satisfy boundary or interface conditions. Generally, on an interface between two linear media (assuming that there are no source on the interface) the following field components

$$\mathbf{E}_{\tan},\ \mathbf{H}_{\tan},\ \mathbf{n} \cdot \mathbf{D}, \quad \text{and} \quad \mathbf{n} \cdot \mathbf{B}, \tag{7}$$

are continuous across the interface. Here $\mathbf{F}_{\tan}$ denotes tangential component of a vector field $\mathbf{F}$ on a surface and $\mathbf{n}$ is the unit normal vector of the surface. On the surface of an ideally conducting object (perfect electric conductor, PEC), the boundary conditions read

$$\mathbf{E}_{\tan} = 0 \quad \text{and} \quad \mathbf{n} \cdot \mathbf{B} = 0. \tag{8}$$

If the conductor is not ideally conducting, it may be modelled with the impedance boundary condition (IBC) [63]

$$\mathbf{E}_{\tan} = \bar{\bar{\mathcal{Z}}}_S \cdot (\mathbf{n} \times \mathbf{H}) \tag{9}$$

where $\bar{\bar{\mathcal{Z}}}_S$ is the surface impedance. It is also possible to write the boundary conditions solely in terms of the normal field components [64, 65].

On unbounded regions the solutions of Maxwell's equations should also satisfy the radiation condition

$$\lim_{|\mathbf{r}|\to\infty} |\mathbf{r}| \left(\eta \mathbf{H}(\mathbf{r}) \times \frac{\mathbf{r}}{|\mathbf{r}|} - \mathbf{E}(\mathbf{r}) \right) = 0, \tag{10}$$

where $\eta = \sqrt{\mu/\varepsilon}$ is the wave impedance of a homogeneous medium.

3.2. Integral Equation Representations

IEMs for finding solutions of Maxwell's equations are based on *equivalence principles*, also known as *integral equation representations*. With these principles the scatterer or other structure is removed and replaced with equivalent sources that radiate the same EM fields as in the original physical problem.

First we assume that a (virtual) surface S encloses a homogeneous and isotropic domain that is characterized with constant and scalar material parameters ε and μ, and that the sources of the primary fields $\mathbf{E}^{\mathrm{p}}$ and $\mathbf{H}^{\mathrm{p}}$ are inside that domain. Then the *surface equivalence principle (SEP)* states that the total fields inside the domain are uniquely determined by the primary fields and the secondary fields expressed in terms of the (rotated) tangential components of the total fields on S. These rotated tangential field components are known as the *equivalent surface current densities*

$$\mathbf{J}_S(\mathbf{r}) = \mathbf{n}(\mathbf{r}) \times \mathbf{H}(\mathbf{r}), \quad \text{and} \quad \mathbf{M}_S(\mathbf{r}) = \mathbf{E}(\mathbf{r}) \times \mathbf{n}(\mathbf{r}), \tag{11}$$

where $\mathbf{n}$ is the unit normal vector of S pointing into the domain in which the field representations are applied.

Next assume that an inhomogeneous and anisotropic object with position dependent dyadic material parameters $\bar{\bar{\varepsilon}}$ and $\bar{\bar{\mu}}$ is embedded in a homogeneous and isotropic medium with constant material parameters ε and μ (not necessarily vacuum). Then the *volume equivalence principle (VEP)* states that the secondary fields, generated as the primary fields interact with the object, can be expressed in terms of the *volume (polarization) current densities*

$$\mathbf{J}_V(\mathbf{r}) = -i\omega\varepsilon \bar{\bar{\tau}}_E(\mathbf{r}) \cdot \mathbf{E}(\mathbf{r}), \quad \text{and} \quad \mathbf{M}_V(\mathbf{r}) = -i\omega\mu \bar{\bar{\tau}}_H(\mathbf{r}) \cdot \mathbf{H}(\mathbf{r}). \tag{12}$$

Here dyadic material contrast functions are given by

$$\bar{\bar{\tau}}_E(\mathbf{r}) = \bar{\bar{\varepsilon}}_r(\mathbf{r}) - \bar{\bar{\mathcal{I}}} \quad \text{and} \quad \bar{\bar{\tau}}_H(\mathbf{r}) = \bar{\bar{\mu}}_r(\mathbf{r}) - \bar{\bar{\mathcal{I}}}, \tag{13}$$

and $\bar{\bar{\mathcal{I}}}$ is the identity dyadic. By introducing a *potential integral operator* (on surfaces this operator is known as the *single layer operator*)

$$\boldsymbol{\mathcal{S}}_\Omega[\mathbf{F}_\Omega](\mathbf{r}) := \int_\Omega G(\mathbf{r}, \mathbf{r}') \mathbf{F}_\Omega(\mathbf{r}') d\Omega', \tag{14}$$

with the homogeneous space Green's function $G(\mathbf{r}, \mathbf{r}') = \exp(ik|\mathbf{r} - \mathbf{r}'|)/(4\pi|\mathbf{r} - \mathbf{r}'|)$ and wavenumber $k = \omega\sqrt{\varepsilon\mu}$, both the SEP and VEP can be mathematically formulated as

$$\Theta(\mathbf{r})\mathbf{E}(\mathbf{r}) = \mathbf{E}^p(\mathbf{r}) - \frac{\eta}{ik} \left(\nabla\nabla\cdot + k^2 \right) \boldsymbol{\mathcal{S}}_\Omega[\mathbf{J}_\Omega](\mathbf{r}) - \nabla \times \boldsymbol{\mathcal{S}}_\Omega[\mathbf{M}_\Omega](\mathbf{r}), \tag{15}$$

$$\Theta(\mathbf{r})\mathbf{H}(\mathbf{r}) = \mathbf{H}^p(\mathbf{r}) - \frac{1}{ik\eta} \left(\nabla\nabla\cdot + k^2 \right) \boldsymbol{\mathcal{S}}_\Omega[\mathbf{M}_\Omega](\mathbf{r}) + \nabla \times \boldsymbol{\mathcal{S}}_\Omega[\mathbf{J}_\Omega](\mathbf{r}). \tag{16}$$

Here Ω is the support of the equivalent sources, either volume V or surface S, and Θ is a function of the field point $\mathbf{r}$. For volume sources, $\Theta(\mathbf{r}) = 1$ for all $\mathbf{r} \in \mathbb{R}^3$ and G is the Green's function of the (homogeneous and isotropic) background medium. For surface sources Θ is defined as

$$\Theta(\mathbf{r}) = \begin{cases} 1 & \text{if} \quad \mathbf{r} \in D, \\ 1/2 & \text{if} \quad \mathbf{r} \in S, \\ 0 & \text{otherwise}, \end{cases} \tag{17}$$

where D is the domain (occupied by S) in which the SEP is formulated and G is the Green's function of that (homogeneous and isotropic) domain.

For later use, let us introduce the following three integral operators

$$\boldsymbol{\mathcal{L}}_\Omega[\mathbf{F}](\mathbf{r}) := \left(\nabla\nabla\cdot + k^2\right)\boldsymbol{\mathcal{S}}_\Omega[\mathbf{F}](\mathbf{r}), \tag{18}$$

$$\boldsymbol{\mathcal{T}}_\Omega[\mathbf{F}](\mathbf{r}) := \nabla\times\nabla\times\boldsymbol{\mathcal{S}}_\Omega[\mathbf{F}](\mathbf{r}), \tag{19}$$

$$\boldsymbol{\mathcal{K}}_\Omega[\mathbf{F}](\mathbf{r}) := \nabla\times\boldsymbol{\mathcal{S}}_\Omega[\mathbf{F}](\mathbf{r}). \tag{20}$$

Similarly as the potential operator $\boldsymbol{\mathcal{S}}$ above, also these operators are defined for both volume and surface sources. For the surface sources these operators are defined as Cauchy principal value integrals if the field point is on the surface. In the following, the currents and operators are denoted without Ω, whenever there is no chance of misinterpretation.

3.3. Surface Integral Equation Formulations

In principal, SIEs can be used in any media where Green's function is known [15, 66], but from a practical implementation point of view the Green's function should have an expression that allows efficient enough numerical evaluations.

We continue by deriving two fundamental SIEs in a homogeneous and isotropic medium that are used to develop alternative SIE formulations. The fields are first expressed using representations (15) and (16). Since these representations give 3D fields in terms of their (2D) rotated tangential components, SIEs are usually derived by taking tangential traces (components) of the field representations on the boundaries. Operating with a *rotated tangential trace operator*

$$\gamma_r\mathbf{F} := \mathbf{n}\times\mathbf{F}|_S, \tag{21}$$

gives the *electric and magnetic current surface integral equation* (JMSIE), also known as the rotated tangential or N-equations [48, 68],

$$\begin{bmatrix} -\gamma_r\boldsymbol{\mathcal{K}} + \frac{1}{2}\boldsymbol{\mathcal{I}} & \frac{\eta}{ik}\gamma_r\boldsymbol{\mathcal{L}} \\ \frac{-1}{ik\eta}\gamma_r\boldsymbol{\mathcal{L}} & -\gamma_r\boldsymbol{\mathcal{K}} + \frac{1}{2}\boldsymbol{\mathcal{I}} \end{bmatrix} \begin{bmatrix} \mathbf{J} \\ \mathbf{M} \end{bmatrix} = \begin{bmatrix} \gamma_r\mathbf{H}^p \\ -\gamma_r\mathbf{E}^p \end{bmatrix}. \tag{22}$$

Here $\boldsymbol{\mathcal{I}}[\mathbf{F}] = \mathbf{F}$ is the identity operator. Another set of equations is obtained with a *tangential trace operator*

$$\gamma_t\mathbf{F} := -\mathbf{n}\times\mathbf{n}\times\mathbf{F}|_S. \tag{23}$$

This gives the *electric and magnetic field surface integral equations* (EHSIE), the tangential or T-equations [48, 68],

$$\begin{bmatrix} \frac{\eta}{ik}\gamma_t\boldsymbol{\mathcal{L}} & -\gamma_t\boldsymbol{\mathcal{K}} - \frac{1}{2}\gamma_r \\ \gamma_t\boldsymbol{\mathcal{K}} - \frac{1}{2}\gamma_r & \frac{1}{ik\eta}\gamma_t\boldsymbol{\mathcal{L}} \end{bmatrix} \begin{bmatrix} \mathbf{J} \\ \mathbf{M} \end{bmatrix} = \begin{bmatrix} \gamma_t\mathbf{E}^p \\ \gamma_t\mathbf{H}^p \end{bmatrix}. \tag{24}$$

† It is important to note that Equations (22) and (24) without the boundary or interface conditions are not solvable. Consider first a penetrable homogeneous and isotropic object D_2 in a homogeneous and isotropic background D_1. Because the tangential field components are continuous across the interface of D_1 and D_2, the current densities on the opposite sides of the interface are equal (up to a sign). Thus, there are only two independent unknowns, one electric and one magnetic. In order to have the same number of unknowns and equations, the number of equations should be reduced, too. This can be done in infinitely many ways. Let us call the equations of (22) the *electric and magnetic current integral equations* of domain D_j, ECIE_j and MCIE_j, and the equations of (24) the *electric and magnetic field integral equations* of domain D_j, EFIE_j and MFIE_j, respectively. All the equations and associated operators $\boldsymbol{\mathcal{L}}_j$ and $\boldsymbol{\mathcal{K}}_j$ are defined with material parameters ε_j, μ_j, and Green's functions G_j of domain D_j, $j = 1, 2$. Then, the equations of D_j are combined into two equations [48, 69]

$$a_j\mathrm{ECIE}_j + b_j\mathrm{EFIE}_j, \tag{25}$$

$$c_j\mathrm{MCIE}_j + d_j\mathrm{MFIE}_j. \tag{26}$$

† We have used unconventional names for integral Equations (22) and (24). Justification of these names is that Equation (22) defines a mapping from the equivalent currents to themselves and Equation (24) defines a mapping from the equivalent currents to the tangential fields.

The choice of the coupling coefficients a_j, b_j, c_j and d_j, $j = 1, 2$, has a significant effect on both theoretical and numerical properties of the resulting SIE formulation. Coefficients of five popular SIE formulations are listed in Table 1 (columns 2–6). Finally, Equations (25) and (26) arising from the opposite sides of an interface are combined leading to two combined equations for two unknowns [48].

Table 1. Coupling coefficients of the surface integral equation formulations.

	CNF	CTF	PMCHWT	NMüller	JMCFIE	PEC/IBC-EFIE	PEC/IBC-MFIE	PEC/IBC-CFIE
a_j	1	0	0	μ_{rj}	1	0	1	1
b_j	0	η_j	1	0	η_j	1	0	η_j
c_j	1	0	0	ε_{rj}	1	0	0	0
d_j	0	$1/\eta_j$	1	0	$1/\eta_j$	0	0	0

For example, the equations of PMCHWT [71] and CNF [48] formulations are as follows (assuming that the primary field have only sources in domain D_1) ‡

$$\begin{bmatrix} \frac{\eta_1}{ik_1}\gamma_t\boldsymbol{\mathcal{L}}_1 + \frac{\eta_2}{ik_2}\gamma_t\boldsymbol{\mathcal{L}}_2 & \gamma_t\boldsymbol{\mathcal{K}}_1 + \gamma_t\boldsymbol{\mathcal{K}}_2 \\ -\gamma_t\boldsymbol{\mathcal{K}}_1 - \gamma_t\boldsymbol{\mathcal{K}}_2 & \frac{1}{ik_1\eta_1}\gamma_t\boldsymbol{\mathcal{L}}_1 + \frac{1}{ik_2\eta_2}\gamma_t\boldsymbol{\mathcal{L}}_2 \end{bmatrix} \begin{bmatrix} \mathbf{J} \\ \mathbf{M} \end{bmatrix} = \begin{bmatrix} \gamma_t\mathbf{E}^p \\ \gamma_t\mathbf{H}^p \end{bmatrix} \tag{27}$$

and

$$\left(\begin{bmatrix} -\gamma_r\boldsymbol{\mathcal{K}}_1 + \gamma_r\boldsymbol{\mathcal{K}}_2 & \frac{1}{ik_1\eta_1}\gamma_r\boldsymbol{\mathcal{L}}_1 - \frac{1}{ik_2\eta_2}\gamma_r\boldsymbol{\mathcal{L}}_2 \\ ik_1\eta_1\gamma_r\boldsymbol{\mathcal{L}}_1 - ik_2\eta_2\gamma_r\boldsymbol{\mathcal{L}}_2 & \gamma_r\boldsymbol{\mathcal{K}}_1 - \gamma_r\boldsymbol{\mathcal{K}}_2 \end{bmatrix} + \begin{bmatrix} \boldsymbol{\mathcal{I}} & 0 \\ 0 & \boldsymbol{\mathcal{I}} \end{bmatrix} \right) \begin{bmatrix} \mathbf{J} \\ \mathbf{M} \end{bmatrix} = \begin{bmatrix} \gamma_r\mathbf{H}^p \\ \gamma_r\mathbf{E}^p \end{bmatrix}. \tag{28}$$

In the case of an impenetrable object, modeled with a mathematical boundary condition, the current and field equations are first derived similarly as above, but only on the background medium. Then one of the unknown currents is usually eliminated via the boundary condition. The last three columns of Table 1 give the coupling coefficients of the three most well-known SIE formulations for the PEC and IBC boundary conditions, assuming that the magnetic current is eliminated from the equations. We note that magnetic equations, MCIE and MFIE, are not used if $\mathbf{M}$ does not appear as an unknown.

The electric field integral equation with the PEC condition reads (PEC-EFIE)

$$\frac{\eta}{ik}\gamma_t\boldsymbol{\mathcal{L}}[\mathbf{J}] = \gamma_t\mathbf{E}^p \tag{29}$$

and the magnetic field integral equation (PEC-MFIE) is §

$$\left(-\gamma_r\boldsymbol{\mathcal{K}} + \frac{1}{2}\boldsymbol{\mathcal{I}}\right)[\mathbf{J}] = \gamma_r\mathbf{H}^p. \tag{30}$$

For the IBC with scalar surface impedance Z_S the IBC-EFIE and IBC-MFIE are [72]

$$\frac{\eta}{ik}\gamma_t\boldsymbol{\mathcal{L}}[\mathbf{J}] - \gamma_t\boldsymbol{\mathcal{K}}\left[Z_S\mathbf{n}\times\mathbf{J}\right] + \frac{Z_S}{2}\mathbf{J} = \gamma_t\mathbf{E}^p, \tag{31}$$

$$\frac{-1}{ik\eta}\gamma_r\boldsymbol{\mathcal{L}}\left[Z_S\mathbf{n}\times\mathbf{J}\right] - \gamma_r\boldsymbol{\mathcal{K}}[\mathbf{J}] + \frac{1}{2}\mathbf{J} = \gamma_r\mathbf{H}^p. \tag{32}$$

A similar procedure as above can be applied for other boundary conditions as well, e.g., for so called DB and $D'B'$ conditions [73, 74]. This, however, results in integral equations and formulations that depend on the boundary condition [53, 73, 74]. Recently, an alternative more general approach is proposed for the IBC [58] — a rather similar idea was proposed about 30 years before [27]. In this approach the integral equations are written for both the electric and magnetic currents and the boundary condition is enforced in the weak sense as an additional equation.

‡ Using the same terminology as above, these equations should be called as coupled field formulation and coupled current formulation, respectively. To avoid further confusion, we have used their old names, PMCHWT and CNF.

§ Using the terminology above, this equation should be called as PEC-ECIE, the electric current integral equation.

The extension of the SIE formulation for multiple non-connected impenetrable or penetrable objects with the same material parameters is rather straightforward. The situation, however, becomes much more involved for connected composite objects with altering materials and/or boundary conditions. The challenge here is an efficient treatment of the "junctions" of the boundaries and interfaces. In [75] a systematic and easy-to-follow approach was proposed to solve the problem.

3.4. Volume Integral Equation Formulations

VIEs are required in cases where the object is truly inhomogeneous and/or anisotropic and Green's functions for the SIEs are not available or feasible. Assume next that D is a bounded domain in $\mathbb{R}^3$ with position depended dyadic material parameters $\bar{\bar{\varepsilon}}$ and $\bar{\bar{\mu}}$, and that D is embedded in a homogeneous and isotropic (background) medium with constant parameters ε and μ. Formulation of the VIEs starts by expressing the total fields with VEP (15) and (16). Depending on the choice of the unknown function alternative formulations can be obtained. First, one can write the volume currents in terms of the electric and magnetic flux densities

$$\mathbf{J} = -i\omega\left(\bar{\bar{\mathcal{I}}} - \bar{\bar{\varepsilon}}_r^{-1}\right)\cdot\mathbf{D} \quad \text{and} \quad \mathbf{M} = -i\omega\left(\bar{\bar{\mathcal{I}}} - \bar{\bar{\mu}}_r^{-1}\right)\cdot\mathbf{B}. \tag{33}$$

Then by multiplying Equation (15) with ε and Equation (16) with μ, we obtain the VIE for the flux densities, the *DBVIE formulation*,

$$\left[\begin{array}{cc} -\boldsymbol{\mathcal{L}}_{\chi_E} + \bar{\bar{\varepsilon}}_r^{-1}\cdot & -i\omega\varepsilon\boldsymbol{\mathcal{K}}_{\chi_H} \\ i\omega\mu\boldsymbol{\mathcal{K}}_{\chi_E} & -\boldsymbol{\mathcal{L}}_{\chi_H} + \bar{\bar{\mu}}_r^{-1}\cdot \end{array}\right]\left[\begin{array}{c} \mathbf{D} \\ \mathbf{B} \end{array}\right] = \left[\begin{array}{c} \mathbf{D}^{\mathrm{p}} \\ \mathbf{B}^{\mathrm{p}} \end{array}\right]. \tag{34}$$

Here $\mathbf{D}^{\mathrm{p}} = \varepsilon\mathbf{E}^p$, $\mathbf{B}^{\mathrm{p}} = \mu\mathbf{H}^p$, $\boldsymbol{\mathcal{A}}_\chi[\mathbf{F}] = \boldsymbol{\mathcal{A}}[\chi\mathbf{F}]$, and

$$\chi_E = \bar{\bar{\mathcal{I}}} - \bar{\bar{\varepsilon}}_r^{-1} \quad \text{and} \quad \chi_H = \bar{\bar{\mathcal{I}}} - \bar{\bar{\mu}}_r^{-1}. \tag{35}$$

A formulation for the field intensities is obtained by using identity [51]

$$\boldsymbol{\mathcal{L}}_V[\mathbf{F}] = \boldsymbol{\mathcal{T}}_V[\mathbf{F}] - \mathbf{F}, \tag{36}$$

and by expressing the volume currents in terms of the fields. The equations of this *EHVIE formulation* read

$$\left[\begin{array}{cc} -\boldsymbol{\mathcal{T}}_{\tau_E} + \bar{\bar{\varepsilon}}_r\cdot & -i\omega\mu\boldsymbol{\mathcal{K}}_{\tau_H} \\ i\omega\varepsilon\boldsymbol{\mathcal{K}}_{\tau_E} & -\boldsymbol{\mathcal{T}}_{\tau_H} + \bar{\bar{\mu}}_r\cdot \end{array}\right]\left[\begin{array}{c} \mathbf{E} \\ \mathbf{H} \end{array}\right] = \left[\begin{array}{c} \mathbf{E}^{\mathrm{p}} \\ \mathbf{H}^{\mathrm{p}} \end{array}\right]. \tag{37}$$

The third option, JMVIE formulation, written in terms of scaled volume currents $\tilde{\mathbf{J}} = \mathbf{J}/\sqrt{\varepsilon}$ and $\tilde{\mathbf{M}} = \mathbf{M}/\sqrt{\mu}$, is given by [57]

$$\left[\begin{array}{cc} \boldsymbol{\mathcal{I}} - \bar{\bar{\tau}}_E\cdot\boldsymbol{\mathcal{L}} & -ik\bar{\bar{\tau}}_E\cdot\boldsymbol{\mathcal{K}} \\ ik\bar{\bar{\tau}}_H\cdot\boldsymbol{\mathcal{K}} & \boldsymbol{\mathcal{I}} - \bar{\bar{\tau}}_H\cdot\boldsymbol{\mathcal{L}} \end{array}\right]\left[\begin{array}{c} \tilde{\mathbf{J}} \\ \tilde{\mathbf{M}} \end{array}\right] = \left[\begin{array}{c} \tilde{\mathbf{J}}^{\mathrm{p}} \\ \tilde{\mathbf{M}}^{\mathrm{p}} \end{array}\right]. \tag{38}$$

Here $\tilde{\mathbf{J}}^{\mathrm{p}} = -i\omega\varepsilon\bar{\bar{\tau}}_E\cdot\tilde{\mathbf{E}}^{\mathrm{p}}$ and $\tilde{\mathbf{M}}^{\mathrm{p}} = -i\omega\mu\bar{\bar{\tau}}_H\cdot\tilde{\mathbf{H}}^{\mathrm{p}}$ with $\tilde{\mathbf{E}}^{\mathrm{p}} = \mathbf{E}^{\mathrm{p}}/\sqrt{\varepsilon}$ and $\tilde{\mathbf{H}}^{\mathrm{p}} = \mathbf{H}^{\mathrm{p}}/\sqrt{\mu}$. Other possible VIE formulations are presented, e.g., in [51, 76].

For a bi-anisotropic medium the VIE representations have exactly the same form as for an anisotropic medium with the difference that the volume currents contain extra terms due to the magneto-electric coupling parameters

$$\mathbf{J} = -i\omega\varepsilon\bar{\bar{\tau}}_E\cdot\mathbf{E} - i\omega\bar{\bar{\xi}}\cdot\mathbf{H} \quad \text{and} \quad \mathbf{M} = -i\omega\mu\bar{\bar{\tau}}_H\cdot\mathbf{H} - i\omega\bar{\bar{\zeta}}\cdot\mathbf{E}. \tag{39}$$

The JMVIE formulation for a bi-anisotropic medium can be expressed as

$$\left[\begin{array}{cc} \boldsymbol{\mathcal{I}} - \bar{\bar{\tau}}_E\cdot\boldsymbol{\mathcal{L}} + ik\bar{\bar{\xi}}_r\cdot\boldsymbol{\mathcal{K}} & -\bar{\bar{\xi}}_r\cdot\boldsymbol{\mathcal{L}} - ik\bar{\bar{\tau}}_E\cdot\boldsymbol{\mathcal{K}} \\ -\bar{\bar{\zeta}}_r\cdot\boldsymbol{\mathcal{L}} + ik\bar{\bar{\tau}}_H\cdot\boldsymbol{\mathcal{K}} & \boldsymbol{\mathcal{I}} - \bar{\bar{\tau}}_H\cdot\boldsymbol{\mathcal{L}} - ik\bar{\bar{\zeta}}_r\cdot\boldsymbol{\mathcal{K}} \end{array}\right]\left[\begin{array}{c} \tilde{\mathbf{J}} \\ \tilde{\mathbf{M}} \end{array}\right] = -i\omega\left[\begin{array}{c} \bar{\bar{\tau}}_E\cdot\tilde{\mathbf{D}}^p + \bar{\bar{\xi}}_r\cdot\tilde{\mathbf{B}}^p \\ \bar{\bar{\tau}}_H\cdot\tilde{\mathbf{B}}^p + \bar{\bar{\zeta}}_r\cdot\tilde{\mathbf{D}}^p \end{array}\right], \tag{40}$$

with $\bar{\bar{\xi}} = \sqrt{\varepsilon\mu}\bar{\bar{\xi}}_r$, $\bar{\bar{\zeta}} = \sqrt{\varepsilon\mu}\bar{\bar{\zeta}}_r$, $\tilde{\mathbf{D}}^{\mathrm{p}} = \sqrt{\varepsilon}\mathbf{E}^p$ and $\tilde{\mathbf{B}}^{\mathrm{p}} = \sqrt{\mu}\mathbf{H}^p$.

If the structure to be modeled contains both penetrable (inhomogeneous and/or anisotropic) and impenetrable regions, coupled volume-surface integral equation (VSIE) formulation is needed. In this formulation the total fields are expressed as a sum of the primary fields and the secondary fields due to both the equivalent surface and volume currents [77].

3.5. Integral Operators and Equations

Consider next a linear integral operator

$$\boldsymbol{\mathcal{A}}[\mathbf{u}](\mathbf{r}) := \int_{\Omega} K(\mathbf{r},\mathbf{r}')\,\mathbf{u}(\mathbf{r}')d\Omega', \tag{41}$$

where $\mathbf{u}$ is an unknown function and K is a known function — the kernel of $\boldsymbol{\mathcal{A}}$. An operator $\boldsymbol{\mathcal{A}}$ can be interpreted as a linear mapping from the domain space $\mathcal{D}$ onto the range space $\mathcal{R}$. Operator is called a smoothing operator if the range space consists of functions that are "smoother" than in the domain space. If the operator decreases the smoothness of a function it acts like a differential operator.

Linear integral operators can be classified due to the singularity of their kernel. If the order of the singularity of the kernel is lower than the dimension of the integral, the kernel is called *weakly singular*. An operator with a weakly singular kernel is smoothing and *bounded*. Spectrum of a bounded operator is bounded in the complex plane. If the spectrum accumulates to the origin, the operator is called *compact*. If the order of the singularity of the kernel is equal or higher than the dimension of the integral, the kernel is *singular or hyper-singular*. Operators with strongly or hyper-singular kernels can be *unbounded* in which case the spectrum tends to go to the infinity.

Integral equations in turn can be classified as *integral equations of the first kind*

$$\boldsymbol{\mathcal{A}}_1[\mathbf{u}] = \mathbf{v}, \tag{42}$$

and as *integral equations of the second kind*

$$(\boldsymbol{\mathcal{A}}_2 + \boldsymbol{\mathcal{I}})\,[\mathbf{u}] = \mathbf{v}, \tag{43}$$

where $\boldsymbol{\mathcal{A}}_1$ and $\boldsymbol{\mathcal{A}}_2$ are linear integral operators. A very important class of integral equations is the Fredholm's integral equations of the second kind — compact plus identity. The mathematical theory of these equations is well-established. They are uniquely solvable if $\boldsymbol{\mathcal{A}}_2 + \boldsymbol{\mathcal{I}}$ is one-to-one and their spectrum accumulates to a constant value in the complex plane. Unfortunately in EM, the integral equations are of this nice form only in some very rare special cases. Generally, for uniquely solvable equations, operators $\boldsymbol{\mathcal{A}}_1$ and $\boldsymbol{\mathcal{A}}_2 + \boldsymbol{\mathcal{B}}$ (this is a generalization of (43)) should be one-to-one, and operator $\boldsymbol{\mathcal{A}}_1$ should be coercive ("bounded from below"), and operator $\boldsymbol{\mathcal{A}}_2$ should be compact and $\boldsymbol{\mathcal{B}}$ should be bounded with a bounded inverse.

3.6. Method of Moments

Method of Moments (MoM) is a general projection method for finding numerical (approximate) solutions of linear (integral) operator equations [78]. With MoM infinite dimensional integral equations are converted to finite dimensional matrix equations

$$\mathbf{A}\mathbf{x} = \mathbf{b}, \tag{44}$$

that can be solved with numerical methods. Here $\mathbf{A}$ is a system matrix, $\mathbf{b}$ is an excitation vector, and vector $\mathbf{x}$ contains the unknown coefficients of the approximation of the unknown function. The basic steps of MoM can be summarized as follows [79]:

(i) Approximate an unknown function $\mathbf{u}$ with a linear combination of known basis functions $\mathbf{u}_1, \ldots, \mathbf{u}_N$

$$\mathbf{u} \approx \sum_{n=1}^{N} c_n \mathbf{u}_n. \tag{45}$$

(ii) Minimize the residual of the approximate equations, obtained by substituting (45) into the integral equation, against known testing or weighting functions $\mathbf{w}_m$, $m = 1, 2, \ldots$.

Assuming that the testing procedure is based on the symmetric L^2 product

$$\langle \mathbf{w},\, \mathbf{v} \rangle := \int_{\Omega} \mathbf{w}(\mathbf{r}) \cdot \mathbf{v}(\mathbf{r}) d\Omega, \tag{46}$$

where Ω is either a volume (V) or a surface (S), the elements of (44) (for an integral equation of the first kind (42)) are

$$A_{mn} = \langle \mathbf{w}_m\,,\, \boldsymbol{\mathcal{A}}_1[\mathbf{u}_n] \rangle\,, \quad b_m = \langle \mathbf{w}_m\,,\, \mathbf{v} \rangle\,, \quad m, n = 1, \ldots, N. \tag{47}$$

3.7. Function Spaces

Next we introduce the mathematical function spaces, *Sobolev spaces*, associated with the analysis of the solutions of the EM integral equations [80]. For the field intensities the natural function space is the space of square integrable functions whose curls are also square integrable [80–82], called here as *curl space*,

$$H_{\text{curl}}(V) := \left\{ \mathbf{F} \,|\, \mathbf{F} \in L^2(V)^3 \quad \text{and} \quad \nabla \times \mathbf{F} \in L^2(V)^3 \right\}. \tag{48}$$

Here $L^2(V)^3$ denotes the space of square integrable (vector) functions and V is a bounded domain in 3D. If V is unbounded, square integrability is defined locally on each bounded subset of V [80]. For the flux densities we define the *div space*

$$H_{\text{div}}(V) := \left\{ \mathbf{F} \,|\, \mathbf{F} \in L^2(V)^3 \quad \text{and} \quad \nabla \cdot \mathbf{F} \in L^2(V) \right\}. \tag{49}$$

Furthermore, as can be deduced from Maxwell's equations (3) and (4), in a source free medium the flux densities are solenoidal (divergence vanishes). Therefore, define a third function space

$$H_{\text{div, sol}}(V) := \left\{ \mathbf{F} \,|\, \mathbf{F} \in H_{\text{div}}(V) \quad \text{and} \quad \nabla \cdot \mathbf{F} = 0 \right\}. \tag{50}$$

These three function spaces (48), (49), and (50), together with $L^2(V)^3$, are the ones needed to analyze the EM VIEs [91].

For the analysis of the SIEs, the trace spaces of the above-mentioned curl and div space are needed [80, 83]. Let S denote the surface of V with unit normal vector $\mathbf{n}$. Then the trace operators introduced in Section 3.3 define the following mappings [82]

$$\gamma_t : \quad H_{\text{curl}}(V) \mapsto H^{-1/2}_{\text{Curl}}(S), \tag{51}$$

$$\gamma_r : \quad H_{\text{curl}}(V) \mapsto H^{-1/2}_{\text{Div}}(S). \tag{52}$$

Here "the surface curl space" and its L^2 dual space, "the surface div space", are defined as

$$H^{-1/2}_{\text{Curl}}(S) : = \left\{ \mathbf{F} \,|\, \mathbf{F} \in H^{-1/2}(S) \quad \text{and} \quad \text{Curl}\, \mathbf{F} \in H^{-1/2}(S) \right\}, \tag{53}$$

$$H^{-1/2}_{\text{Div}}(S) : = \left\{ \mathbf{F} \,|\, \mathbf{F} \in H^{-1/2}(S) \quad \text{and} \quad \text{Div}\mathbf{F} \in H^{-1/2}(S) \right\}. \tag{54}$$

Operations Curl $\mathbf{F} = \mathbf{n} \cdot \nabla_s \times \mathbf{F}$ and Div$\mathbf{F} = \nabla_s \cdot \mathbf{F}$ are the *surface curl* and *surface divergence* of a tangential vector field defined on the surface. Space $H^{-1/2}(S)$ is the L^2 dual of the fractional order scalar Sobolev space $H^{1/2}(S)$ [80]. Spaces (53) and (54) are the ones used to analyze properties of the SIEs expressed in terms of the surface current densities. For SIEs containing surface charge densities

$$\rho = \mathbf{n} \cdot \mathbf{D} \quad \text{and} \quad \zeta = \mathbf{n} \cdot \mathbf{B}, \tag{55}$$

a normal trace operator

$$\gamma_n \mathbf{F} := \mathbf{n} \cdot \mathbf{F}|_S \tag{56}$$

is needed. This trace operator defines the following mapping

$$\gamma_n : H_{\text{div}}(V) \mapsto H^{-1/2}(S). \tag{57}$$

and $H^{-1/2}(S)$ is the function space for the surface charge densities.

4. ACCURATE, STABLE AND SCALABLE SOLUTIONS

The previous section provides background for the EM IEMs. Next we turn our attention to the properties of various formulations and equations. We, in particular, look for methodologies that would lead to accurate, stable, and scalable solutions on a wide range of material parameters and frequencies.

4.1. Accuracy

Accuracy is the first fundamental property of any numerical method. It depends on many factors such as modeling of the geometry and materials, approximation of the unknown function, accuracy of numerical evaluations, e.g., numerical integration, and solution of the linear system [84]. We consider two issues related to the accuracy of the solution: Numerical evaluation of singular integrals with the singularity subtraction technique (SST) and choices of the basis and testing functions that lead to conforming discretization strategies.

4.1.1. Evaluation of Singular Integrals

The kernels of the integral operators become singular as the field and source points coincide. In EM the kernels are defined with the Green's function, its derivatives, and in some VIEs with additional material parameter depended functions. Green's function has a weak $O(1/R)$ singularity as $R = |\mathbf{r} - \mathbf{r}'| \to 0$. Differentiating the Green's function increases the order of the singularity. Gradient of the Green's function has a $O(1/R^2)$ singularity that for surface integrals leads to a strongly singular kernel that generally is not integrable. For the surface integral operator $\boldsymbol{\mathcal{L}}_S$, having a strongly singular kernel, the order of the singularity can be reduced by moving gradient from the singular Green's function to a differentiable testing function by integrating by parts

$$\langle \mathbf{w}, \boldsymbol{\mathcal{L}}_S[\mathbf{J}_S] \rangle = - \langle \mathrm{Div}\, \mathbf{w}, \boldsymbol{\mathcal{S}}_S[\mathrm{Div}\, \mathbf{J}_S] \rangle + k^2 \langle \mathbf{w}, \boldsymbol{\mathcal{S}}_S[\mathbf{J}_S] \rangle . \tag{58}$$

It is important to note that this form is valid only if a testing function $\mathbf{w}$ has a correct differentiability property (divergence conforming, see the next section).

For volume integrals gradient of the Green's function still defines a weakly singular kernel, but double derivative leads to a strongly singular one. In the latter case, the singularity can be decreased by moving one of the derivatives to the testing function. The difference compared to (58) is that for VIEs similar nice symmetric variational form does not usually exist and we need to consider boundary integrals, too. For example, for the operator $\boldsymbol{\mathcal{L}}_V$, appearing in the JMVIE formulation and tested with a L^2 conforming function $\mathbf{w}$, we have [57]

$$\langle \mathbf{w}, \bar{\bar{\tau}}_E \cdot \boldsymbol{\mathcal{L}}_V[\mathbf{J}_V] \rangle = - \left\langle \nabla \cdot \left(\bar{\bar{\tau}}_E^T \cdot \mathbf{w} \right), \nabla \boldsymbol{\mathcal{S}}_V[\mathbf{J}_V] \right\rangle + \int_{\partial V} \mathbf{n} \cdot \left(\bar{\bar{\tau}}_E^T \cdot \mathbf{w} \right) \cdot \nabla \boldsymbol{\mathcal{S}}_V[\mathbf{J}_V] dS + k^2 \langle \mathbf{w}, \bar{\bar{\tau}}_E \cdot \boldsymbol{\mathcal{S}}_V[\mathbf{J}_V] \rangle . \tag{59}$$

Here ∂V denotes the boundary of V and $\mathbf{n}$ is the unit normal vector of ∂V.

However, it is not possible to avoid all singularities and special techniques are still required to obtain satisfactory accuracy. After discretizing SIEs and VIEs with MoM one has to consider, for example, the following types of double integrals (omitting possible vector and material parameter functions)

$$\int_\Omega \int_\Omega P_m^{(q)}(\mathbf{r}) P_m^{(p)}(\mathbf{r}') G(\mathbf{r}, \mathbf{r}') d\Omega' d\Omega, \quad \text{and} \quad \int_\Omega \int_\Omega P_m^{(q)}(\mathbf{r}) P_m^{(p)}(\mathbf{r}') \nabla G(\mathbf{r}, \mathbf{r}') d\Omega' d\Omega. \tag{60}$$

Here $P_m^{(q)}$ and $P_m^{(p)}$ are polynomials of orders p and q (related to the testing and basis functions).

The idea in SST is to subtract and add singular term(s) from the kernel [85, 86]. By expanding the exponential function with the power series homogeneous space Green's function can be expressed as

$$G(R) = \sum_{p=0}^{\infty} \frac{(ik)^p R^{p-1}}{4\pi p!} = \frac{1}{4\pi R} - \frac{k^2 R}{8\pi} + O(R^2), \quad R \neq 0. \tag{61}$$

Then by subtracting and adding every second term up to order four gives

$$G(R) = \left(G(R) - \sum_{p=0,2,4} \frac{(ik)^p R^{p-1}}{4\pi p!} \right) + \sum_{p=0,2,4} \frac{(ik)^p R^{p-1}}{4\pi p!}. \tag{62}$$

The terms with odd p are not usually considered since they are smooth functions. The terms on the right-most of (62) can be evaluated analytically on planar polygons and the remaining term on the right hand side of (62) is usually sufficiently smooth to allow numerical integration with standard techniques [87, 88]. It is important to note that subtracting only one term may not be enough since the function to be evaluated numerically may not be smooth enough and for strongly singular integrals usually at least three terms should be subtracted from the kernel [87].

It is also important to note that with the SST presented here it is not possible to obtain arbitrary accuracy (with finite number of quadrature points). In many practical cases including planar elements the accuracy of SST, however, is sufficient. Curved elements still pose major challenges for SST, and other methods based, e.g., on the singularity cancellation method [89] or the direct evaluation method [90] can allow much easier treatment of singular integrals in those cases. Finally, we note that methods like Duffy's transformation does not usually give satisfactory accuracy, in particular, for SIEs with strongly singular kernels and for the VIEs in the case of high material contrast [51].

4.1.2. Conforming Discretization Techniques

Accuracy of the MoM solution depends strongly on the choices of the basis and testing functions. A wrong choice of these functions may deteriorate the accuracy and lead to non-converging solutions. In order to guarantee that the MoM solution converges in the norm of the numerical solution space, with the testing procedure of (46), requires finding the basis functions from the finite dimensional subspace of the domain of an integral operator and the testing functions from the dual of the range space of the operator [91, 92]. This leads to *conforming discretization strategies*. A finite element (FE) space is said to be H *conforming* if it is a finite dimensional subspace of a function space H [82] and a discretization strategy is said to be conforming if both the basis and testing FE spaces are conforming.

In order to find out the needed conforming FE spaces, the domain and range spaces of the associated integral operators need to be known. The volume integral operators introduced in Section 3.4 define the following mappings [57]

$$\text{DBVIE}: \quad H_{\text{div}}(V) \times H_{\text{div}}(V) \;\mapsto\; H_{\text{curl}}(V) \times H_{\text{curl}}(V), \tag{63}$$

$$\text{EHVIE}: \quad H_{\text{curl}}(V) \times H_{\text{curl}}(V) \;\mapsto\; H_{\text{div}}(V) \times H_{\text{div}}(V), \tag{64}$$

$$\text{JMVIE}: \quad L_2(V)^3 \times L_2(V)^3 \;\mapsto\; L_2(V)^3 \times L_2(V)^3. \tag{65}$$

Recall that $H_{\text{div}}(V)$ and $H_{\text{curl}}(V)$ are L^2 dual spaces to each other and that $L^2(V)^3$ is its own dual. Then results (63) through (65) show that in order to use conforming discretization strategies so that the operators become tested in the dual of their range spaces, the FE spaces of the basis and testing functions for all three VIEs considered here should be identical. For DBVIE one should use H_{div} *(divergence) conforming* functions, for EHVIE we need H_{curl} *(curl) conforming* functions, and for JMVIE L^2 conforming functions. These functions differ by their continuity properties [82]. Divergence conforming functions, such as SWG functions [93], have continuous normal component across the faces of the mesh, curl conforming Nedelec's edge functions [94] have continuous tangential component from an element to another and $L^2(V)$ conforming functions do not pose any continuity between the elements. In other words, these functions have the same continuity properties as the corresponding physical quantities (flux, field and current) approximated with these functions.

The surface integral operators derived in Section 3.3 define the mappings [56]

$$\text{JMSIE}: \quad H_{\text{Div}}^{-1/2}(S) \times H_{\text{Div}}^{-1/2}(S) \;\mapsto\; H_{\text{Div}}^{-1/2}(S) \times H_{\text{Div}}^{-1/2}(S), \tag{66}$$

$$\text{EHSIE}: \quad H_{\text{Div}}^{-1/2}(S) \times H_{\text{Div}}^{-1/2}(S) \;\mapsto\; H_{\text{Curl}}^{-1/2}(S) \times H_{\text{Curl}}^{-1/2}(S). \tag{67}$$

Since $H_{\text{Div}}^{-1/2}(S)$ is the L^2 dual of $H_{\text{Curl}}^{-1/2}(S)$, EHSIE should be discretized with $H_{\text{Div}}^{-1/2}$ (divergence) conforming basis and testing functions, but for the JMSIE only the basis functions should be divergence conforming, and the testing functions should be $H_{\text{Curl}}^{-1/2}$ (curl) conforming. The difference here is that a divergence conforming function has continuous component perpendicular to the edges of the mesh and well-defined surface divergence, whereas a curl conforming function has a continuous component parallel to the edges of the mesh and well-defined surface curl.

If the lowest order divergence conforming FE space, i.e., the RWG [25] space, is used as the basis function space for JMSIE, the curl conforming FE space obtained by operating with $\mathbf{n}\times$ to the RWG space, can not be used as the testing function space. The reason is that these two spaces do not define an appropriate non-degenerate L^2 dual pairing [95]. Instead, another curl conforming FE space, a *dual curl conforming* space, is needed. This space may for example consists of the rotated tangential Buffa-Christiansen functions [96]. Conforming discretization techniques utilizing above-mentioned FE spaces are summarized in Table 2.

Table 2 shows an important fundamental result. Conventionally, in CEM the integral equations have been discretized using Galerkin's method with identical basis and testing functions. This method,

Table 2. Conforming discretization strategies for the volume and surface integral equations.

	DBVIE	EHVIE	JMVIE	JMSIE	EHSIE
Basis FE space	div conf.	curl conf.	L^2 conf.	div conf.	div conf.
Testing FE space	div conf.	curl conf.	L^2 conf.	dual curl conf.	div conf.

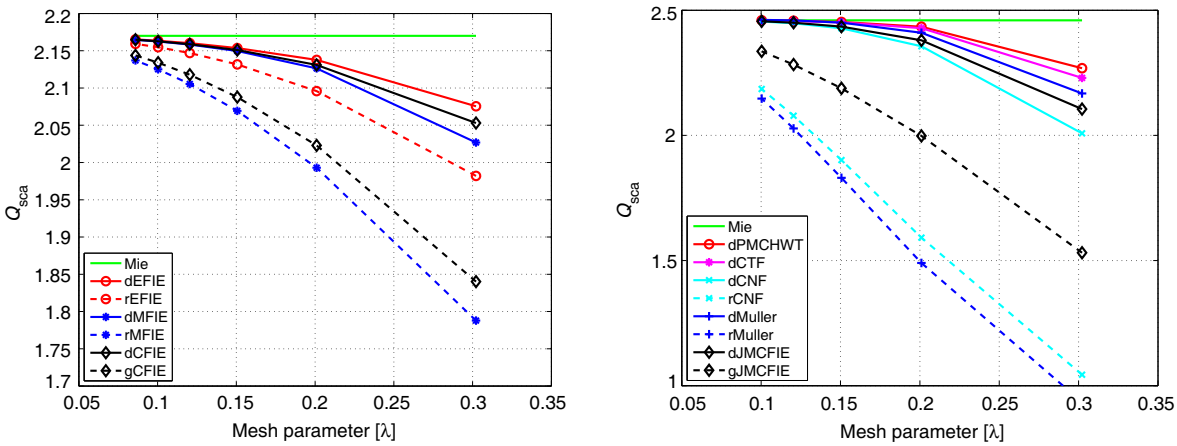

Figure 1. Total scattering versus the mesh parameter (average edge length): (a) a PEC sphere with $r = \lambda/2$ and (b) a homogeneous dielectric sphere with $r = \lambda/2$ and $\varepsilon_r = 4$. Here d stands for testing in the dual of the range space (conforming), r for testing in the range space (non-conforming) and g for testing with Galerkin's method (in CFIE and JMCFIE the field equations are tested in the dual of their range spaces, but the current equations are tested in the range spaces). In all cases basis functions are the RWG functions.

as indicated by Table 2, gives conforming discretization strategy for all other formulations except for the JMSIE. Consequently, using standard RWG-Galerkin approaches for equations based on JMSIE, such as PEC-MFIE, CNF and NMüller, may not guarantee that the solution converges in the norm of the numerical solution, i.e., in the $H_{\text{Div}}^{-1/2}(S)$ norm. In particular, the solution for the charge may not converge [54, 97]. Figure 1 illustrates that conforming strategies (denoted with solid lines) give much faster converging solutions than the non-conforming ones (denoted with dashed lines).

The rationale why testing in the dual of the range space is important can be found by studying the Helmholtz decompositions of the testing function spaces. Consider first testing of the DBVIE. Define the following (incomplete) Helmholtz decomposition (the harmonic part is removed) for the volumetric divergence conforming testing function space

$$\mathbf{w}_V^{\text{div}} = \nabla \times \mathbf{w}_V + \mathbf{w}_V^{\text{nsol}}. \tag{68}$$

Here $\nabla \times \mathbf{w}_V$ is a solenoidal, and $\mathbf{w}_V^{\text{nsol}}$ is a non-solenoidal function. Since DBVIE defines a mapping from the flux densities onto the field intensities, consider testing of the electric field with a divergence conforming function having decomposition (68). Integrating by parts gives

$$\begin{aligned}\left\langle \mathbf{w}_V^{\text{div}}, \mathbf{E} \right\rangle &= \left\langle \nabla \times \mathbf{w}_V + \mathbf{w}_V^{\text{nsol}}, \mathbf{E} \right\rangle = \langle \mathbf{w}_V, \nabla \times \mathbf{E} \rangle - \langle \mathbf{w}_V, \gamma_r \mathbf{E} \rangle_S + \left\langle \mathbf{w}_V^{\text{nsol}}, \mathbf{E} \right\rangle \\ &= i\omega \langle \mathbf{w}_V, \mathbf{B} \rangle - \langle \mathbf{w}_V, \gamma_r \mathbf{E} \rangle_S + \left\langle \mathbf{w}_V^{\text{nsol}}, \mathbf{E} \right\rangle. \end{aligned} \tag{69}$$

This shows that by testing the DVIE part of the DBVIE in the dual of its range space, tests both the electric field and its curl, i.e., the magnetic flux, inside the volume, and the tangential component of the electric field on the interfaces. Analogously, testing the BVIE part of the DBVIE in the dual of its range space, tests both the magnetic field and the electric flux inside the volume, and the tangential component of the magnetic field on the interfaces. If the equations are not tested in the dual of the range space, the flux densities may not be tested properly and their solutions may not converge.

With similar arguments, and using Helmholtz decomposition of a curl conforming testing function space, it can be shown that testing the equations of EHVIE in the dual of their range spaces tests the flux densities and the fields inside the volume, and the normal components of the fluxes on the interfaces. If the equations are not tested in the dual of the range space, the field intensities may not be tested.

Consider next the surface formulations. Testing the tangential electric field with the Helmholtz decomposition of the divergence conforming testing function space

$$\mathbf{w}_S^{\mathrm{div}} = \mathbf{n} \times \nabla_s \phi + \mathbf{w}_S^{\mathrm{nsol}}, \tag{70}$$

where $\mathbf{n} \times \nabla_s \phi$ is a solenoidal function and $\mathbf{w}_S^{\mathrm{nsol}}$ is a non-solenoidal function, gives

$$\begin{aligned} \left\langle \mathbf{w}_S^{\mathrm{div}},\, \gamma_t \mathbf{E} \right\rangle &= \left\langle \mathbf{n} \times \nabla_s \phi + \mathbf{w}_S^{\mathrm{nsol}},\, \gamma_t \mathbf{E} \right\rangle = \langle \phi,\, \mathrm{Div}\, \mathbf{M} \rangle + \left\langle \mathbf{w}_S^{\mathrm{nsol}},\, \gamma_t \mathbf{E} \right\rangle \\ &= i\omega \langle \phi,\, \gamma_n \mathbf{B} \rangle + \left\langle \mathbf{w}_S^{\mathrm{nsol}},\, \gamma_t \mathbf{E} \right\rangle. \end{aligned} \tag{71}$$

This shows that by testing the EFIE part of the EHSIE in the dual of its range space, tests the boundary or interface conditions for both the tangential electric field and the normal magnetic flux. Analogously, utilizing Helmholtz decomposition of a curl conforming testing function space shows that testing the ECIE (rotated tangential component of the magnetic field) part of the JMSIE in the dual of its range tests both the electric surface current density and its divergence [97]. If the operators are not tested in the dual of their range spaces, the normal components of flux densities may not be tested in the EHSIE and the surface divergence of the currents may not be tested in the JMSIE, and the convergence of the solution for these non-tested field quantities is not guaranteed.

4.2. Stability

The formulations and their conforming discretizations considered so far do not necessarily guarantee that the resulting matrix equation is stable and well-conditioned. Generally, stability is related to the condition number of the matrix, *measure of the sensitivity of the linear system.* If the condition number of a matrix is high, the system is usually ill-conditioned and small changes on the initial conditions may cause large changes on the solution.

Another very important issue related to the conditioning of a matrix is the convergence rate of iterative solutions. For efficient iterative solutions with Krylov subspace methods a matrix should be sufficiently well-conditioned. Strictly speaking, only Fredholm's integral equation of the second kind can lead to a well-conditioned matrix [98]. In all other cases additional regularization or preconditioning techniques may be needed. Next we investigate stability of the VIE and SIE formulations and their regulatization.

4.2.1. Analysis of the Volume Formulations

Consider first properties of the volume formulations (34), (37), and (38). First we note that among these three formulations only the JMVIE is of the form — an integral operator plus the identity operator. In the other two formulations, DBVIE and EHVIE, the identity operator is multiplied with material parameters.

To guarantee that the volume formulations are well-posed, the material parameters should be bounded from both below and above [91, 92]. For example, the electric permittivity should satisfy

$$a \langle \mathbf{F}^*,\, \mathbf{F} \rangle \leq |\langle \mathbf{F}^*,\, \varepsilon \mathbf{F} \rangle| \leq b \langle \mathbf{F}^*,\, \mathbf{F} \rangle \tag{72}$$

for some $0 < a,\, b < \infty$, and for any $\mathbf{F} \in L^2(V)^3$. Here $\mathbf{F}^*$ denotes complex conjugate. Obviously, at the limiting cases $\varepsilon \to 0$ and $\varepsilon \to \infty$ these conditions are not valid. Consequently, the VIE formulations may not be equivalent in the sense of the existence and uniqueness of the solution, and numerical stability issues might arise when approaching these limits. In particular, as discussed in [91], the standard discretization procedures used in the EHVIE and DBVIE might give rise to larger solution spaces as the intended ones.

From the physical point of view, the constitutive relations $\mathbf{D} = \varepsilon \mathbf{E}$, and $\mathbf{B} = \mu \mathbf{H}$, and the finite energy assumption, indicate the following about the flux densities and the fields at the limiting cases:

$$\lim_{\varepsilon \to 0} \mathbf{D} = 0, \quad \lim_{\mu \to 0} \mathbf{B} = 0, \quad \lim_{\varepsilon \to \infty} \mathbf{E} = 0, \quad \lim_{\mu \to \infty} \mathbf{H} = 0. \tag{73}$$

Obviously these limiting cases cause numerical problems for the formulations using the fields or fluxes as unknowns. The equivalent volume currents $\mathbf{J}$ and $\mathbf{M}$ are linear combinations of the fluxes and fields

and do not vanish in the limiting cases. The stability of the JMVIE formulation is illustrated in Figure 2 for a radially anisotropic sphere.

As is mentioned in Section 3.7, in a source free medium the flux densities should have zero divergence. To satisfy this, the basis functions used to approximate the flux densities should be solenoidal [99]. Figure 2 shows that, compared to the standard discretization of DBVIE with SWG functions, the use of solenoidal functions stabilizes DBVIE at small permittivity values, but the condition number of the matrix is increases on other values. By defining the solenoidal loop functions with projections, as proposed in [47] for surface formulations, improves conditioning of the matrix. This, however, requires inversion of the Gram matrix whose efficient computation can be challenging.

Nonetheless, the standard discretization of the DBVIE formulation with Galerkin's method and SWG functions might give convergent results in the L^2 norm. However, it is not clear that the divergence of the flux density converges inside the scatterer. As illustrated in Figure 3, with the solenoidal functions the solution of the DBVIE has an equal converge rate both in the L^2 and $H_{\rm div}$ norms.

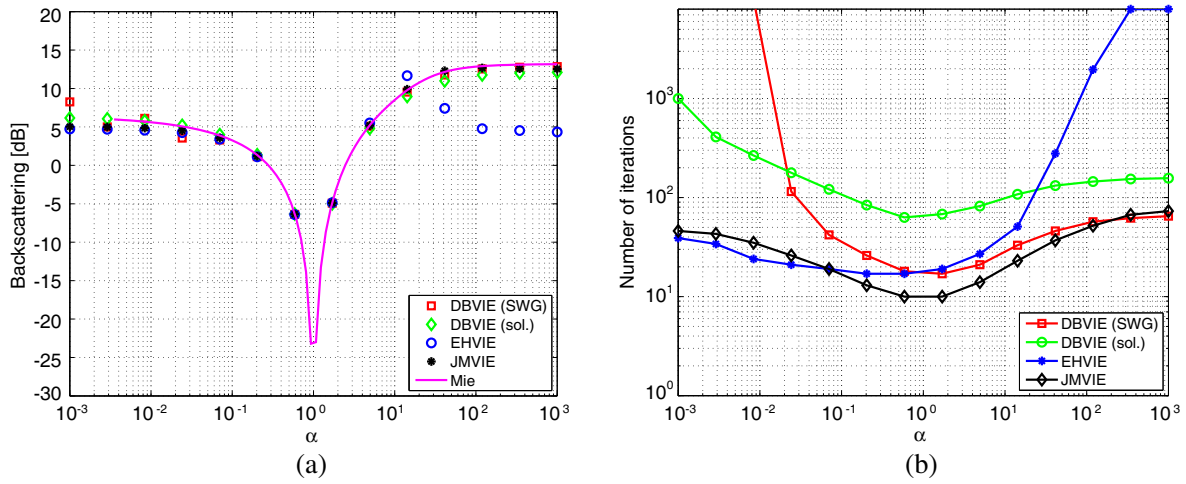

Figure 2. (a) Backscattered RCS and (b) the number of GMRES iterations of various VIE formulations versus the radial component of the permittivity and permeability dyadics of a sphere with size parameter $kr = 2$. Here k is the wavenumber of the background (vacuum) and sol. stands for the solenoidal basis and testing functions.

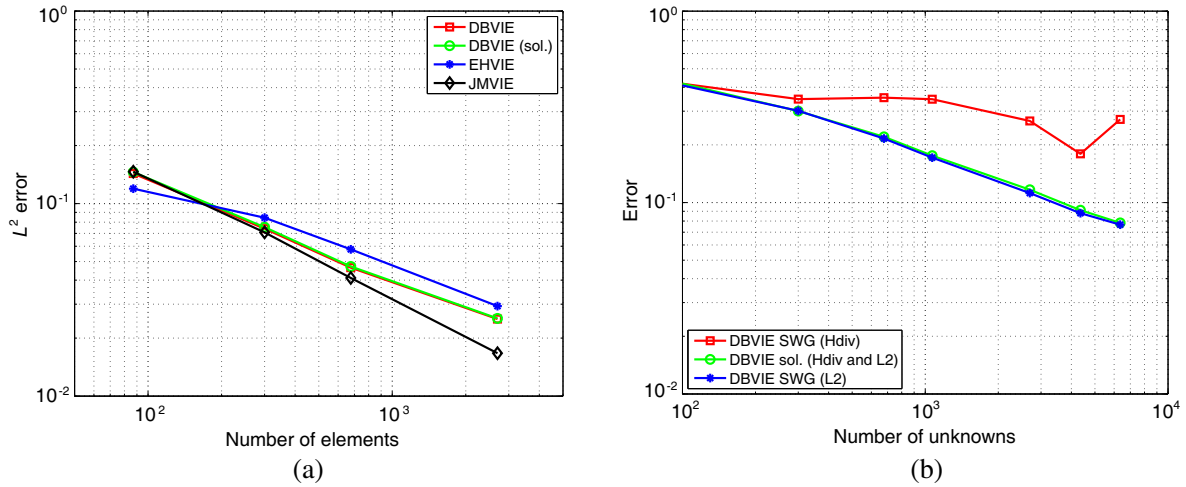

Figure 3. (a) Relative error in the total scattering cross section for different VIE formulations and (b) the accuracy of the solution of the DBVIE formulation inside the object using various norms. In both cases the object is a dielectric ($\varepsilon_r = 5$) sphere of size $kr = 2$.

4.2.2. Material Parameter Regularization of Volume Formulations

Another problem related to the VIEs is that the condition number of the matrix tends to increase as the material contrast of the object is increased. In order to avoid this, we consider a Helmholtz decomposition based preconditioner for the JMVIE in the case of a homogeneous isotropic object with $\varepsilon = \varepsilon_r \varepsilon_0$ and $\mu = \mu_0$ [100].

Any vector field $\mathbf{F} \in L^2(V)^3$ can be decomposed using Helmholtz decomposition into the irrotational, solenoidal and gradient of harmonic parts [101]

$$\mathbf{F} = \nabla P + \nabla \times \mathbf{w} + \nabla H, \tag{74}$$

where $P \in H_0^1(V)$, $\mathbf{w} \in H_{\mathrm{curl}_0}(V)$, and H is a harmonic function with zero Laplacian in V. Here

$$H^1(V) := \left\{ u \,|\, u \in L^2(V) \quad \text{and} \quad \nabla u \in (L^2(V))^3 \right\} \tag{75}$$

is the classical Sobolev space of square integral functions whose first derivatives are also square integrable, and index 0 stands for vanishing functions in V $(H_0^1(V))$ or for vanishing tangential components on the boundary of V $(H_{\mathrm{curl}_0}(V))$. According to (74), electric volume current $\mathbf{J}$ can be decomposed as

$$\mathbf{J} = \mathbf{J}_{\mathrm{sol}} + \mathbf{J}_{\mathrm{irr}} + \mathbf{J}_{\mathrm{harm}}. \tag{76}$$

Since inside the volume $\nabla \cdot \mathbf{J}_{\mathrm{sol}} = 0$, and on the boundary $\mathbf{n} \cdot \mathbf{J}_{\mathrm{sol}} = 0$, JMVIE for the solenoidal part reduces to

$$\mathbf{J}_{\mathrm{sol}} - \tau_E k_0^2 \boldsymbol{\mathcal{S}}[\mathbf{J}_{\mathrm{sol}}] = \mathbf{J}^p. \tag{77}$$

If $\tau_E = \varepsilon_r - 1$ is bounded, Equation (77) is of the desired form, identity plus compact, and its spectrum accumulates to unity.

To analyze the irrotational part we use identity (36) and write JMVIE as

$$\varepsilon_r \mathbf{J} - \tau_E \boldsymbol{\mathcal{T}}[\mathbf{J}] = \mathbf{J}^p. \tag{78}$$

Now operator $\boldsymbol{\mathcal{T}}$ vanishes since $\nabla \times \mathbf{J}_{\mathrm{irr}} = 0$ and on the boundary $\mathbf{n} \times \mathbf{J}_{\mathrm{irr}} = 0$. Thus, only the permittivity and the identity operators act on the irrotational part, and the accumulation point of the spectrum is at ε_r.

Finally, substituting the gradient of the harmonic function, $\mathbf{J}_{\mathrm{harm}} = \nabla H$, into the JMVIE, integrating by parts, and using the fact that Laplacian of H vanishes, gives [100]

$$\mathbf{J}_{\mathrm{harm}} + \tau_E \nabla \boldsymbol{\mathcal{S}}[\gamma_n \mathbf{J}_{\mathrm{harm}}] - k_0^2 \boldsymbol{\mathcal{S}}[\mathbf{J}_{\mathrm{harm}}] = \mathbf{J}^p. \tag{79}$$

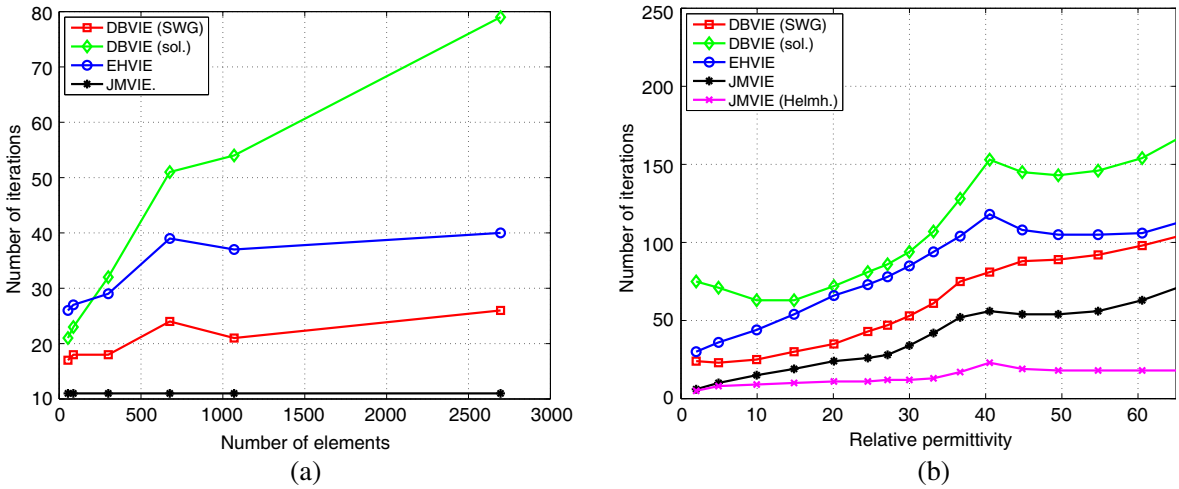

Figure 4. The number of GMRES iterations versus the number of elements for a sphere with (a) $kr = 1$ and $\varepsilon_r = 5$ and versus the permittivity of a sphere with (b) $kr = 0.4$. Here (Helmh.) stands for the Helmholtz decomposition of the volume current. At $\varepsilon_r = 40$ the increase in the GMRES iterations is due to a physical resonance of a dielectric sphere.

Here γ_n is the normal trace operator (56). Equation (79) is of the form identity plus bounded plus compact. If the boundary ∂V is smooth, the equation can be reduced to the form identity plus compact with an accumulation point $(\varepsilon_r + 1)/2$.

In conclusion, this analysis indicates that the spectrum of the JMVIE operator depends on the material parameter, which may have a negative effect on the stability of the numerical solution. This also indicates that JMVIE is solvable in $L^2(V)$ if $\varepsilon_r \neq 0$ or $\varepsilon_r \neq -1$ and explains why convergence of iterative solvers tend to slow down as the material contrast is increased. Even more importantly the analysis shows that an efficient preconditioner is obtained by scaling the JMVIE in the irrotational subspace by $1/\varepsilon_r$ and in the harmonic subspace by $(\varepsilon_r + 1)/2$ [100].

Figure 4 illustrates that the conditioning of the JMVIE formulation is clearly less dependent on the mesh density than that of the other VIE formulations, and in particular that after regularization via the Helmholtz decomposition, the conditioning of JMVIE is nearly independent on the permittivity contrast, when implemented using similar projection operators as in [47].

4.2.3. Analysis of the Surface Formulations

Consider next properties of the surface formulations. First we note the fundamental difference between equations JMSIE and EHSIE, namely only the first one can lead to integral equations of the second kind, since the second one contains the rotation operator $\mathbf{n}\times$ rather than the identity operator.

With the PEC boundary condition PEC-EFIE (29) is an integral equation of the first kind and PEC-MFIE (30) is an integral equation of the second kind. However, none of these two equations is of the desired form that would generally guarantee uniquely solvable solutions. Firstly, they both fail to be one-to-one at internal Maxwell resonance frequencies of a closed object. This problem can be avoided, e.g., with the PEC-CFIE [23]. Secondly, due to the infinite dimensional null-space of the Div operator within the $\boldsymbol{\mathcal{L}}$ operator, the corresponding variational form (58) or the operator itself is not coercive [95]. Using Helmholtz decomposition the null-space of the Div operator can be extracted and a coercive variational form can be obtained [102]. In addition, if the surface is non-smooth, the $\boldsymbol{\mathcal{K}}$ operator of PEC-MFIE is bounded, rather than compact.

In the case of penetrable bodies the equations arising from the opposite sides of an interface are combined. This complicates the analysis of the formulations and certain specific choices of the coupling coefficients leads to cancellations in the combined equations, that has significant effects on the properties

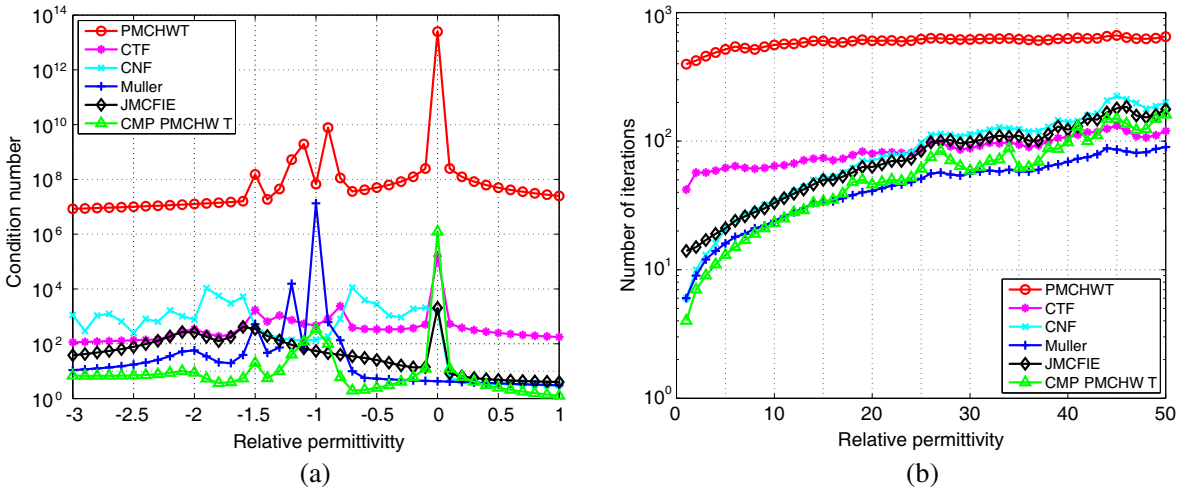

Figure 5. Eigenvalue condition numbers (ratio of the maximum and minimum magnitudes of the eigenvalues) of various SIE formulations versus the relative permittivity of a homogeneous dielectric sphere with (a) $kr = 1$ and the number of GMRES iterations (without restarts and additional preconditioning) needed to obtain relative residual error of 10^{-4} versus the relative permittivity of a homogeneous dielectric cube with (b) $kL = 2$. CMP-PMCHWT stands for the Calderon matrix multiplicative preconditioned PMCHWT formulation and L is the edge length of a cube.

of the formulations. In the PMCHWT formulation the rotation operators cancel, leading to an integral equation of the first kind. The mathematical analysis of this formulation is considered, e.g., in [103]. In the NMüller formulation the equations are coupled so that the main singularity of the $\boldsymbol{\mathcal{L}}$ operator cancels [104] and the resulting equation is of the second kind — bounded plus identity. This cancellation, however, may have a negative effect on the near field accuracy. CTF is a scaled version of PMCHWT where the diagonal blocks of the system matrix are identical. This significantly improves conditioning of the matrix, with the cost of non-vanishing rotation operators. CNF is an integral equation of the second kind that is based on the same JMSIE equations as the NMüller formulation, but without any additional scaling coefficients nor cancellations.

As illustrated in Figure 5, an additional challenge in the SIE formulations for penetrable objects is that the conditioning of the matrix tends to increase as the material contrast is increased. As can be deduced from (27) and (28), the reason for this is that the matrix blocks (in PMCHWT the diagonal ones and in CNF the off-diagonal ones) become more and more ill-balanced as the material contrast is increased. Thus, additional scaling of the equations, and/or normalization of the unknowns [106], may still be needed to avoid growth of the condition number with respect to the material parameters. As shown also in Figure 5, for certain specific material parameters the integral equations can become singular, or fail to give correct results [61, 105]. Particularly problematic cases seem to be material parameter values of zero or minus one.

4.2.4. Low Frequency Stability of Surface Formulations

Surface formulations suffer also from the low frequency breakdown — a consequence of decoupling of the electric and magnetic fields at zero frequency [42]. To illustrate this problem, decompose operator $\boldsymbol{\mathcal{L}}$, multiplied with a coefficient as, e.g., in the PEC-EFIE (29), in two parts as

$$\frac{-1}{i\omega\varepsilon}\boldsymbol{\mathcal{L}} = \boldsymbol{\mathcal{L}}^h + \boldsymbol{\mathcal{L}}^s \tag{80}$$

with

$$\left(\boldsymbol{\mathcal{L}}^h\,\mathbf{F}\right) = \frac{-1}{i\omega\varepsilon}\nabla\boldsymbol{\mathcal{S}}[\operatorname{Div}\mathbf{F}] \quad \text{and} \quad (\boldsymbol{\mathcal{L}}^s\mathbf{F}) = i\omega\mu\boldsymbol{\mathcal{S}}[\mathbf{F}]. \tag{81}$$

Clearly operators $\boldsymbol{\mathcal{L}}^h$ and $\boldsymbol{\mathcal{L}}^s$ have different frequency scaling. As ω goes to zero, $\boldsymbol{\mathcal{L}}^h$ becomes dominant and the system becomes unbalanced and numerically unstable, because the contribution from $\boldsymbol{\mathcal{L}}^s$ is lost and the current can not be accurately determined from its divergence. This results in a nearly singular matrix at low frequencies and a singular matrix at zero frequency [107–109]. The low frequency breakdown appears in all SIEs containing the $\boldsymbol{\mathcal{L}}$ operator. Particularly problematic are the PEC-EFIE, PMCHWT and CTF formulations, where the $\boldsymbol{\mathcal{L}}$ operator has a dominant role in the sense that it is "well-tested". Due to the cancellation of the hyper-singular part of the $\boldsymbol{\mathcal{L}}$ operator, the NMüller formulation is a low frequency stable formulation [110]. CNF suffers from the low-frequency problem, but the problem is not as severe, since the problematic $\boldsymbol{\mathcal{L}}$ operator is weakly tested [48].

The usual method to regularize SIEs at low frequencies is based on the *incomplete surface Helmholtz decomposition* of the currents [42, 111]. With proper frequency scaling this decomposition leads to a solvable matrix equation at low frequencies. The challenge, however, still is that the resulting matrix is typically very poorly conditioned due to unbounded form of the Helmholtz decomposed operator [42, 112].

Another way to avoid the low-frequency breakdown is to consider charges as independent unknowns. This formulation, giving *current and charge integral equations* (CCIE), is based on representations [49]

$$\Theta\mathbf{E} \;=\; \mathbf{E}^p + i\omega\mu\boldsymbol{\mathcal{S}}[\mathbf{J}] - \boldsymbol{\mathcal{K}}[\mathbf{M}] - \frac{1}{\varepsilon}\nabla\boldsymbol{\mathcal{S}}[\rho], \tag{82}$$

$$\Theta\mathbf{H} \;=\; \mathbf{H}^p + i\omega\varepsilon\boldsymbol{\mathcal{S}}[\mathbf{M}] + \boldsymbol{\mathcal{K}}[\mathbf{J}] + \frac{1}{\mu}\nabla\boldsymbol{\mathcal{S}}[\zeta], \tag{83}$$

where $\rho = \mathbf{n}\cdot\mathbf{D}$ and $\zeta = \mathbf{n}\cdot\mathbf{B}$ are the electric and magnetic *surface charge densities*. Charge densities are related to the current densities via the continuity equations

$$i\omega\rho = \operatorname{Div}\mathbf{J} \quad \text{and} \quad i\omega\zeta = \operatorname{Div}\mathbf{M}. \tag{84}$$

Study next the static limit of representations (82) and (83). As $\omega \to 0$ we get

$$\Theta\mathbf{E} = \mathbf{E}^p - \boldsymbol{\mathcal{K}}_0[\mathbf{M}] - \frac{1}{\varepsilon}\nabla\boldsymbol{\mathcal{S}}_0[\rho], \tag{85}$$

$$\Theta\mathbf{H} = \mathbf{H}^p + \boldsymbol{\mathcal{K}}_0[\mathbf{J}] + \frac{1}{\mu}\nabla\boldsymbol{\mathcal{S}}[\zeta], \tag{86}$$

where $\boldsymbol{\mathcal{K}}_0$ and $\boldsymbol{\mathcal{S}}_0$ are the $\boldsymbol{\mathcal{K}}$ and $\boldsymbol{\mathcal{S}}$ operators with the static Green's function $G_0 = 1/(4\pi|\mathbf{r}-\mathbf{r}'|)$. At zero frequency currents $\mathbf{J}$ and $\mathbf{M}$ are purely solenoidal [42] and can be expressed as

$$\mathbf{M} = -\mathbf{n}\times\mathbf{E} = \mathbf{n}\times\nabla_s\phi \quad \text{and} \quad \mathbf{J} = \mathbf{n}\times\mathbf{H} = \mathbf{n}\times\nabla_s\psi. \tag{87}$$

Using this, and identity [113],

$$\boldsymbol{\mathcal{K}}_0\left[\mathbf{n}\times\nabla_s\phi\right] = -\nabla\boldsymbol{\mathcal{D}}_0[\phi], \tag{88}$$

representation for the electric field (85) at zero frequency reduces to

$$\Theta\mathbf{E} = \mathbf{E}^p + \nabla\boldsymbol{\mathcal{D}}_0[\phi] - \frac{1}{\varepsilon}\nabla\boldsymbol{\mathcal{S}}_0[\rho]. \tag{89}$$

Here $\boldsymbol{\mathcal{D}}_0$ is the double layer potential operator with the static kernel, defined with Green's function G as

$$\boldsymbol{\mathcal{D}}[u](\mathbf{r}) := \int_S \frac{\partial G(\mathbf{r},\mathbf{r}')}{\partial n(\mathbf{r}')}u(\mathbf{r}')dS'. \tag{90}$$

Equation (89) agrees with the representation of the static electric field derived from the representation of the Laplace equation for the electrostatic potential ϕ and its normal derivative $\partial\phi/\partial n = \rho/\varepsilon$. This shows that the static limit of the surface integral representation given in terms of the currents and charges is correct, provided that (87) is satisfied. To ensure that, however, requires explicit use of the surface Helmholtz decomposition.

Next we introduce a modified version of the CCIE formulation [114]. First, write incomplete Helmholtz decompositions of the currents as [111]

$$\mathbf{M} = \mathbf{n}\times\nabla_s\phi + \mathbf{M}^{\text{nsol}} \quad \text{and} \quad \mathbf{J} = \mathbf{n}\times\nabla_s\psi + \mathbf{J}^{\text{nsol}}, \tag{91}$$

where ϕ and ψ are potential functions [111], $\mathbf{J}^{\text{nsol}}$ and $\mathbf{M}^{\text{nsol}}$ are non-solenoidal (surface divergence is non-zero). Since divergence of a solenoidal component is zero, we have

$$\operatorname{Div}\mathbf{M} = \operatorname{Div}\mathbf{M}^{\text{nsol}} = i\omega\zeta \quad \text{and} \quad \operatorname{Div}\mathbf{J} = \operatorname{Div}\mathbf{J}^{\text{nsol}} = i\omega\rho. \tag{92}$$

Then define a *non-solenoidal to charge transformation operator* $\mathbf{W}$ [42, 111], and express the non-solenoidal currents in terms of the charges

$$\mathbf{J} = \mathbf{n}\times\nabla_s\psi + i\omega\mathbf{W}\rho \quad \text{and} \quad \mathbf{M} = \mathbf{n}\times\nabla_s\phi + i\omega\mathbf{W}\zeta. \tag{93}$$

Substituting (93) into field representations (15) and (16), and using identities [115]

$$\boldsymbol{\mathcal{S}}\left[\mathbf{n}\times\nabla_s\phi\right] = -\boldsymbol{\mathcal{K}}[\mathbf{n}\phi] \quad \text{and} \quad \boldsymbol{\mathcal{K}}\left[\mathbf{n}\times\nabla_s\phi\right] = -\boldsymbol{\mathcal{T}}[\mathbf{n}\phi], \tag{94}$$

gives the EM surface integral representations given in terms of four scalar functions, potentials ϕ, ψ, and charges ρ, ζ,

$$\Theta\mathbf{E} = \mathbf{E}^p - \frac{1}{\epsilon}\boldsymbol{\mathcal{T}}[\mathbf{W}\rho] + i\omega\mu\boldsymbol{\mathcal{K}}[\mathbf{n}\psi] + \boldsymbol{\mathcal{T}}[\mathbf{n}\phi] - i\omega\mu\boldsymbol{\mathcal{K}}[\mathbf{W}\zeta], \tag{95}$$

$$\Theta\mathbf{H} = \mathbf{H}^p + \frac{1}{\mu}\boldsymbol{\mathcal{T}}[\mathbf{W}\zeta] - i\omega\varepsilon\boldsymbol{\mathcal{K}}[\mathbf{n}\phi] - \boldsymbol{\mathcal{T}}[\mathbf{n}\psi] + i\omega\varepsilon\boldsymbol{\mathcal{K}}[\mathbf{W}\rho]. \tag{96}$$

Further, with identities [115]

$$\boldsymbol{\mathcal{T}}[\mathbf{W}\rho] = \nabla\boldsymbol{\mathcal{S}}[\rho] + k^2\boldsymbol{\mathcal{S}}[\mathbf{W}\rho] \quad \text{and} \quad \boldsymbol{\mathcal{T}}[\mathbf{n}\phi] = -\nabla\boldsymbol{\mathcal{D}}[\phi] + k^2\boldsymbol{\mathcal{S}}[\mathbf{n}\phi], \tag{97}$$

Equations (95) and (96) at the static limit reduce to

$$\Theta\mathbf{E} = \mathbf{E}^p - \frac{1}{\epsilon}\nabla\boldsymbol{\mathcal{S}}_0[\rho] + \nabla\boldsymbol{\mathcal{D}}_0[\phi], \tag{98}$$

$$\Theta\mathbf{H} = \mathbf{H}^p + \frac{1}{\mu}\nabla\boldsymbol{\mathcal{S}}_0[\zeta] - \nabla\boldsymbol{\mathcal{D}}_0[\psi]. \tag{99}$$

Since these equations agree exactly with the representations of the static fields given in terms of the scalar potentials and their normal derivatives, the SIEs, called as *potential and charge integral equations*, derived from representations (95) and (96) have correct static limit without any additional techniques.

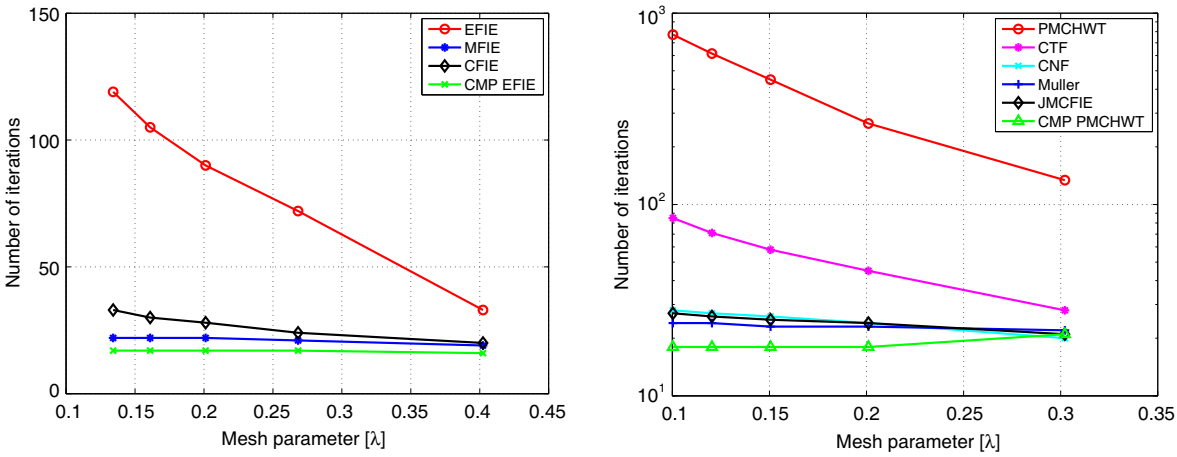

Figure 6. The number of GMRES iterations (without restarts and additional preconditioning) versus the mesh density for a PEC cube with edge length (a) $L = \lambda$ and for a homogeneous dielectric sphere with (b) $r = \lambda/2$. Here CMP-EFIE and CMP-PMCHWT stand for the Calderon matrix multiplicative preconditioned PEC-EFIE and PMCHWT formulations, respectively.

4.2.5. Dense-Mesh Breakdown of Surface Formulations

Another problem of the SIE formulations is the dense-mesh breakdown. The matrix equation becomes more and more ill-conditioned as the mesh density is increased, making iterative solutions ineffective in cases that require discretizations with small elements or elements with varying sizes. The dense-mesh breakdown is associated to the hypersingular part of the operator $\boldsymbol{\mathcal{L}}$ — the gradient of the single layer operator $\nabla\boldsymbol{\mathcal{S}}[u]$. In fact, since $\boldsymbol{\mathcal{L}}$ contains two parts, a hypersingular one $\boldsymbol{\mathcal{L}}^h$ and a compact one $\boldsymbol{\mathcal{L}}^s$, if discretized with the RWG functions, the eigenvalue spectrum of the matrix due to $\boldsymbol{\mathcal{L}}$ scales like $O(1/h^2)$ [112], where h is the mesh parameter. Figure 6 illustrates the dense-mesh breakdown of various SIE formulations. It is important to note that the low frequency and the dense-mesh breakdowns are not the same phenomenon [112] and that the low frequency stable formulations considered in the previous section may still suffer from the dense-mesh breakdown.

Recently, a very elegant technique has been introduced to avoid the dense-mesh breakdown [45]. This technique, called *Calderon preconditioning* [43, 45, 95, 96], is based on the *Calderon integral identity* [80]

$$\left(\frac{-1}{ik}\,\gamma_r\,\boldsymbol{\mathcal{L}}\right)^2 = (\gamma_r\boldsymbol{\mathcal{K}})^2 - \frac{1}{4}\boldsymbol{\mathcal{I}}. \tag{100}$$

This indicates that by multiplying the problematic operator $\gamma_r\boldsymbol{\mathcal{L}}$ with itself results to another operator — the right hand side of (100) — that on smooth surfaces is of the form compact plus identity and on non-smooth surfaces of the form bounded plus identity. By building the preconditioner based on this identity leads to a matrix with bounded spectrum independently on the mesh density. Calderon preconditioner removes also the low frequency breakdown, possibly excluding very low frequencies [116].

The challenge in Calderon preconditioning is to find a discretization strategy that satisfies the nice properties of the continuous equation. With improper discretizations the preconditioned matrix can be even more ill-conditioned than the original one. The crucial requirement for the needed FE spaces is that the square of the hyper-singular part of the $\boldsymbol{\mathcal{L}}$ operator should vanish. We note that using only the familiar RWG space does not satisfy this property, and another dual FE space is required [45, 96]. Another challenge in the discretization of the Calderon preconditioner is that with the RWG and BC Helmholtz decompositions, required at low frequencies [116], the Gram matrix becomes very ill-conditioned [47].

Calderon preconditioning has been successfully applied to regularize ill-conditioned PEC-EFIE formulation and to solve many challenging EM problems [45]. By combining Calderon preconditioned

PEC-EFIE properly with PEC-MFIE, a Calderon preconditioned PEC-CFIE can be obtained [117]. This formulation is both well-conditioned and free of internal resonances. Calderon preconditioning has also been used to regularize PMCHWT formulation in the case of homogeneous isotropic and chiral objects [118, 119].

4.3. Scalability

Still another fundamental problem appears in the IEMs. Namely the CPU time and the computer memory required to solve the matrix equation increase very rapidly as the number of dof is increased. This is due to the fact that discretization of an integral equation leads to a dense matrix equation. The solution time of direct integral equation solvers scales as $O(N^3)$ and the memory consumption as $O(N^2)$, where N is the number of dof required to obtain sufficiently accurate solution. With iterative Krylov subspace methods the CPU time can be reduced to $N_{\text{iter}}O(N^2)$, where N_{niter} is the number of iterations required for the matrix equation to convergence. Still, these numbers are prohibitively high for problems with high number of dof and special acceleration techniques are required to solve large-scale problems with integral equation-based solvers. Next we discuss an error-controllable and efficient broadband MLFMA based on global interpolators and multipole expansions [120].

4.3.1. Broadband MLFMA

MLFMA [37–39] is a versatile and powerful technique to reduce the high computational cost of integral equation-based solvers. Traditionally MLFMA has separate algorithms for the static (low frequency) and dynamic (high frequency) cases. The high frequency version is routinely applied for computing scattering by electrically large structures [29], such as an aircraft, but its application to complex antenna geometries, or other structures with a lot of geometrical details that are small compared with the wavelength, is much more challenging. The low frequency version based on for example multipole expansions of the field components [121], on the other hand, becomes inefficient at higher frequencies since the number of terms required in the expansions increases rapidly as the frequency is increased. Further in such implementation the out-to-in -translation is not diagonal, which makes this operation relatively costly. So the fundamental problem is that neither of these two versions of MLFMA does work efficiently simultaneously in the low and high frequency regimes, or in the cases when the structure contains a lot of electrically small details.

The standard high frequency MLFMA usually works relatively well for both SIEs and VIEs, if the element size of the mesh is not smaller than $\lambda/10$. However, the relevant difference between SIEs and VIEs is that for VIEs the mesh density inside the object should follow the wavelength, whereas as in SIEs one only needs to model surface fields, rather than interior fields. When the contrast of the object is increased the wavelength inside the object becomes shorter, and therefore more elements are required to model the unknown field quantities. This in turn means that the element size inside the body may be significantly below the $\lambda/10$ limit, where λ is the wavelength of the background medium [122].

Next we briefly discuss a broadband version of MLFMA that can be applied on arbitrary mesh densities and frequencies. This algorithm is based on a hybrid multipole expansion-plane wave expansion approach. The idea is to use traditional MLFMA for division cubes larger or equal one lambda ("super-wavelength levels"). In these levels the translation is performed with the standard Rokhlin translator [36]

$$T_L\left(\hat{\mathbf{k}}, \mathbf{D}\right) = \frac{ik}{(4\pi)^2} \sum_{n=0}^{L} i^n (2n+1) h_n^{(1)}(kD) P_n\left(\hat{\mathbf{D}} \cdot \hat{\mathbf{k}}\right), \tag{101}$$

and the Green's function can be represented with a plane-wave expansion

$$G(\mathbf{D}+\mathbf{d}) = \int_S T_L(\hat{\mathbf{k}}, \mathbf{D}) e^{ik\hat{\mathbf{k}}\cdot\mathbf{d}} dS(\hat{\mathbf{k}}), \tag{102}$$

where S is a unit sphere. For division cubes smaller than λ ("sub-wavelength levels") we use a low frequency stable plane wave expansion translator [123, 124]

$$T\left(\hat{\mathbf{k}}, \mathbf{D}\right) = \frac{ik}{8\pi^2} e^{ik\hat{\mathbf{k}}\cdot\mathbf{D}}, \tag{103}$$

and the Green's function is expressed using the spectral representation (for $+z$ direction only, i.e., for $\mathbf{e}_z \cdot (\mathbf{D} + \mathbf{d}) > 0$, the other directions are obtained by rotation [125])

$$G(\mathbf{D} + \mathbf{d}) = \int_{-\pi}^{\pi} \int_{\Gamma} T\left(\hat{\mathbf{k}}, \mathbf{D}\right) e^{ik\hat{\mathbf{k}}\cdot\mathbf{D}} \sin\theta \, d\varphi \, d\theta. \tag{104}$$

The path Γ consists of two parts on the complex θ-plane, namely *the propagating part* from 0 to $\pi/2$ along the positive real axis and the *evanescent part* from $\pi/2$ to $\pi/2 - i\infty$. In the propagating part the direction dependency can be embedded directly into the translator. This makes the switch from the spectral translator to the Rokhlin translator straightforward on the super-wavelength levels, since both can utilize exactly the same planewave expansion of the field components. However, for the evanescent part the radiation and receiving field patterns are expressed in our implementation with multipole expansions to avoid storing six separate planewave expansions, and converted into planewave representation for application of the evanescent part of spectral translator, see (103).

4.3.2. MLFMA with Global Interpolators

Of all the various parts of MLFMA, interpolation is one of the most vital step in the actual implementation of the algorithm. It is of utmost importance that the accuracy can be maintained, and that the method remains efficient while the data is aggregated and disaggregated from an level to another. The available interpolators can be classified as belonging to either *local* or *global* type.

Local interpolators are typically based on Lagrange interpolating polynomials [6, 37, 38]. They allow system matrix-vector multiplication to take place with the asymptotically favourable $O(N \log N)$ CPU-time cost, but unfortunately also require oversampling of the radiation pattern. The fact that these patterns exist on the surface of a unit sphere has not been fully taken advantage of in the existing implementations, and therefore the sample point distribution, especially on the polar regions, is not optimal. Also in practice the obtainable accuracy can be rather limited [126, 127].

One alternative for local interpolators is the global interpolator based on trigonometric polynomial expansions [120, 128, 129]. Such presentations have several useful properties: Conversion between sample values and coefficients of the expansion can be performed effectively and accurately with fast Fourier transform (FFT). Interpolation of a function sampled in a certain set of points can be performed with relative simple zero-padding operation for the corresponding coefficients. Polar regions that complicate implementation of the local interpolation schemes, can be considered trivially by extending functions to 2π-periodic also terms of θ-coordinate. The orthogonality property of the trigonometric polynomial terms guarantees that the accuracy and stability of the process can be maintained even during high number of successive interpolations.

The considered global interpolator also allows the storage of the sampled radiation pattern components to take place in significantly reduced size compared to other alternatives. The version presented in [120] reduced the number of sample points to roughly half compared to the original version [128] by simply reducing the sample rate in the polar regions in φ-direction. Numerical experiments have demonstrated excellent achievable accuracy considering the whole chain: aggregation, out-to-in translation and disaggregation, including the numerical integration over the surface of the unit sphere. Figure 7 illustrates solutions (acoustic surface pressure) of broadband MLFMA (scalar Helmholtz SIE solver) utilizing global interpolators at two frequencies 2.5 Hz and 2.5 kHz corresponding to 22 MHz and 2.2 GHz in EM with the same wavelength as in acoustics. The major challenges of the discussed global interpolator, along with the higher asymptotic cost $O(N \log^2 N)$ [129], are that the construction of the translators is a heavy process and implementation in distributed computing system is challenging.

To avoid the above mentioned drawbacks of the global interpolator without sacrificing its main benefits, in [130] a new version of MLFMA that combines Lagrange interpolating polynomial based local interpolator and the global interpolator utilizing trigonometric polynomial expansions in the same algorithm was proposed. This algorithm combines the best of both approaches: It allows storage of components of radiation patterns with a small number of samples, and should also make it possible to develop an efficient version for distributed computing systems. The key innovation is the developed

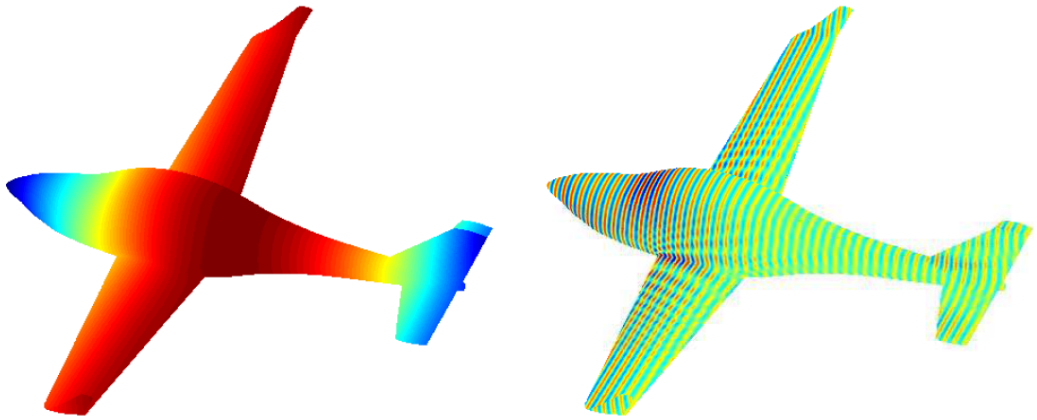

(a) (b)

Figure 7. Acoustic surface pressure at (a) 2.5 Hz and (b) 2.5 kHz computed with the broadband MLFMA utilizing global interpolators. The model includes 1 889 812 planar triangles.

anterpolation process for the global interpolator, which is the standard process in disaggregation with MLFMA utilizing local interpolator based on Lagrange interpolating polynomials.

5. CONCLUSIONS AND FUTURE PERSPECTIVES

During the last three decades there has been an enormous effort in the electrical engineering community to simulate a large variety of EM phenomena using numerical methods. Advanced and sophisticated algorithms and software have been developed to solve complex and challenging problems. In IEMs the discovery of the RWG functions [25] made it possible to developed general solvers for arbitrarily shaped 3D geometries. Fast solvers, like FMM and MLFMA [6, 36], extended significantly the size of the problem that can be solved with the IEMs. Distributed memory parallel implementations further enlarged the size of the problem [131, 132].

Despite of the developments in numerical algorithms and the enormous growth of the computational power there still remain many challenging EM problems whose simulations are inefficient or may even be impossible with existing methods. Matrix equations rising from discretizations can be extremely large and ill-conditioned, and thus difficult to solve even with the most efficient and advanced fast solvers, preconditioners, parallel algorithms and supercomputers. Particularly arduous are the simulations of large and complex multi-domain structures containing small details. An approach, that has already been applied with great success, also in the context of IEMs [133–135], is the domain decomposition method (DDM). This method essentially isolates the solution of one region from another. It may significantly improve the matrix conditioning, and provides an inherent aptitude for parallelization and hybridization of IEMs with other more approximate methods, like physical and geometrical optics, that are required to solve high frequency problems. DDM also provides a natural interface for multi-physics modeling.

There is still a pressing need to develop better formulations, discretization strategies and preconditioning techniques that lead to well-conditioned systems and error-controllable solutions on a wide range of frequencies, materials, geometries and applications [61]. There is both theoretical [91, 92] and numerical [57, 100] evidence that the VIEs, in particular the one written in terms of the volume currents, JMVIE, when discretized correctly, gives stable and accurate solutions on a wide range of material parameters and frequencies, and is also free of the dense-mesh breakdown. Additional regularization, e.g., with Helmholtz decomposition [100], may still be needed to reduce the number of iterations for high contrast materials. Poor conditioning of the system matrix is a particularly serious problem with the SIEs. Many of the present SIE formulations suffer from low frequency and dense-mesh breakdowns, making iterative solutions with Krylov subspace methods ineffective. Calderon preconditioning [45, 96] is one of the most elegant and promising techniques to avoid these problems. So far Calderon preconditioning is available only for PEC and homogeneous dielectric objects modelled with specific integral equation formulations and its generalization for other formulations and boundary

conditions is still an open question. Physical resonances, strongly resonating structures and interior problems pose additional challenges for the preconditioners.

Most often the EM simulators are still used as verification tools, rather than early stage design tools, or their usage is based on simple trial-and-error type simulations, rather than on advanced optimization algorithms. With the growth of computational power and advanced EM simulation tools, it would be beneficial to extend the trial-and-error type simulations of individual parameters to optimizing the comprehensive performance of a device. This requires combination of mathematical optimization techniques with 3D EM full-wave solvers [136, 137], such as IEMs [138, 139] or MLFMA [140]. It would also be beneficial, not only have a solution for a particular problem, but also to have an estimate how accurate the solution is. The user should be able define an error threshold of the solution.

Novel and forthcoming technologies and applications do not only offer grand opportunities, but also pose major challenges for numerical and computational methods. The ever increasing complexity of radio frequency, wireless, microwave and other electronic devices has and will significantly increase requirements for the numerical simulations tools. Numerical methods should be extremely flexible and robust with adjustable accuracy. By utilizing them one should be able to solve complex multi-scale, multi-domain and multi-physics problems on a broad frequency range in near real time. It is not sufficient just to solve one type of problem once, at one frequency, but one needs to be able to solve several different kinds of complex problems several times over wide frequency bands. The present methods need to be generalized, extended for new application areas, and completely new solutions needs to be found. In conclusion, a lot of research and methodology development is still needed until the ultimate goal of *fully error-controllable and near real-time automatic EM design* on a broad range of materials and frequencies is achieved.

ACKNOWLEDGMENT

This work is supported by Academy of Finland, grants No. 259950 entitled Computational and Mathematical Models for Electromagnetic Wave Interaction with Complex Material Structures (COMMA), and No. 259737 entitled Mathematical Optimization Methods for Multiple-Antenna Technologies (MOMMAT), and by the ERC Advanced Grant No. 320773 entitled Scattering and Absorption of Electromagnetic Waves in Particulate Media (SAEMPL).

REFERENCES

1. Williams, L. and S. Rousselle, "EM at the core of complex microwave system design," *IEEE Microwave Magazine*, 97–104, Dec. 2008.
2. Weiland, T., M. Timm, and I. Munteanu, "A practical guide to 3-D simulation," *IEEE Microwave Magazine*, 62–75, Dec. 2008.
3. Maxwell, J. C., *A Treatise of Electricity and Magnetism*, Clarendon Press, Oxford, 1873.
4. Heavyside, O., "On electromagnetic waves, especially in relation to the vorticity of the impressed forces, and the forced vibration of electromagnetic systems," *Philos. Mag.*, Vol 25, 130–156, 1888.
5. Chew, W. C., M. S. Tong, and B. Hu, *Integral Equation Methods for Electromagnetic and Elastic Waves*, Morgan & Claypool Publishers, 2009.
6. Chew, W. C., J.-M. Jin, E. Michielssen, and J. Song, *Fast and Efficient Algorithms in Computational Electromagnetics*, Artech House, Boston, 2001.
7. Volakis, J. L., A. Chatterjee, and L. C. Kempel, *Finite Element Method for Electromagnetics*, IEEE Press, New York, 1998.
8. Jin, J., *The Finite Element Method in Electromagnetics*, John Wiley & Sons, New York, 2002.
9. Zhu, Y. and A. C. Cangellaris, *Multigrid Finite Element Methods for Electromagnetic Field Modeling*, IEEE Press, John Wiley & Sons, New Jersey, 2006.
10. Yee, K. S., "Numerical solution of initial boundary value problems involving Maxwell's equations in isotropic media," *IEEE Trans. Antennas Propag.*, Vol. 14, No. 3, 302–307, 1966.

11. Taflove, A., *Computational Electrodynamics, The Finite-difference Time-domain Method*, Artech House, Boston, 1995.
12. Gedney, S. D., *Introduction to the FDTD Method for Electromagnetics*, Morgan & Claypool, 2011.
13. Kolundzija, B. M. and A. R. Djordjevic, *Electromagnetic Modeling of Composite Metallic and Dielectric Structures*, Artech House, Boston, 2002.
14. Volakis, J. L. and K. Sertel, *Integral Equation Methods for Electromagnetics*, Scitech Publishing, Inc., 2012.
15. Chew, W. C., *Wave and Fields in Inhomogeneous Media*, IEEE Press, New York, 1990.
16. Stratton, J. A. and L. J. Chu, "Diffraction theory of electromagnetic waves," *Physical Review*, Vol. 56, 99–107, 1939.
17. Mei, K. K. and J. G. van Bladel, "Scattering by perfectly conducting rectangular cylinders," *IEEE Trans. Antennas Propag.*, Vol. 11, No. 2, 185–192, Mar. 1963.
18. Andreasen, M. G., "Scattering from parallel metallic cylinders with arbitrary cross section," *IEEE Trans. Antennas Propag.*, Vol. 12, No. 6, 746–754, Nov. 1964.
19. Richmond, J. H., "Scattering by a dielectric cylinder of arbitrary cross-section shape," *IEEE Trans. Antennas Propag.*, Vol. 13, No. 3, 338–341, May 1965.
20. Mei, K. K., "On the integral equations for thin wire antennas," *IEEE Trans. Antennas Propag.*, Vol. 13, No. 3, 374–378, May 1965.
21. Richmond, J. H., "Scattering by an arbitrary array of parallel wires," *IEEE Trans. Microw. Theory Techn.*, Vol. 13, No. 4, 408–412, May 1965.
22. Wu, T. K. and L. L. Tsai, "Scattering from arbitrarily-shaped lossy dielectric bodies of revolution," *Radio Science*, Vol. 12, No. 5, 709–718, 1977.
23. Mautz, J. R. and R. F. Harrington, "H-field, E-field and combined-field solutions for conducting bodies of revolution," *Arch. Elektron. Übertragungstechn. (Electron. Commun.)*, Vol. 32, 157–164, 1978.
24. Mautz, J. R. and R. F. Harrington, "Electromagnetic scattering from a homogeneous material body of revolution," *Arch. Elektron. Übertragungstechn. (Electron. Commun.)*, Vol. 33, 71–80, 1979.
25. Rao, S. M., D. R. Wilton, and A. W. Glisson, "Electromagnetic scattering by surfaces of arbitrary shape," *IEEE Trans. Antennas Propag.*, Vol. 30, No. 3, 409–418, 1982.
26. Umashankar, K., A. Taflove, and S. A. Rao, "Electromagnetic scattering by arbitrary shaped three-dimensional homogeneous lossy dielectric objects," *IEEE Trans. Antennas Propag.*, Vol. 34, No. 6, 758–766, 1986.
27. Medgyesi-Mitschang, L. N., J. M. Putnam, and M. B. Gedera, "Generalized method of moments for three-dimensional penetrable scatterers," *J. Opt. Soc. America, A*, Vol. 11, 1383–1398, Apr. 1994.
28. Glisson, A. W., "Electromagnetic scattering with impedance boundary conditions," *Radio Science*, Vol 27, No. 6, 935–943, 1992.
29. Chew, W. C., H. Y. Chao, T. J. Cui, C. C. Lu, S. Ohnuki, Y. C. Pan, J. M. Song, S. Velamparambil, and J. S. Zhao, "Fast integral equation solvers in computational electromagnetics," *Eng. Anal. Boundary Elem.*, Vol. 27, 803–823, 2003.
30. Sarkar, T. K., E. Arvas, and S. M. Rao, "Application of FFT and the conjugate gradient method for the solution of electromagnetic radiation from electrically large and small conducting bodies," *IEEE Trans. Antennas Propag.*, Vol. 34, No. 5, 635–640, 1986.
31. Peters, T. J. and J. L. Volakis, "Application of a conjugate gradient FFT method to scattering from thin planar material plates," *IEEE Trans. Antennas Propag.*, Vol. 36, No. 4, 518–526, 1988.
32. Zwamborn, A. P. M. and P. M. van den Berg, "Computation of electromagnetic fields inside strongly inhomogeneous objects by the weak-conjugate-gradient fast-Fourier-transform method," *J. Opt. Soc. Am. A*, Vol. 11, 1414–1420, 1994.
33. Gan, H. and W. C. Chew, "A discrete BCG-FFT algorithm for solving 3D inhomogeneous scattering problems," *Journal of Electromagnetic Waves and Applications*, Vol. 9, No. 10, 1339–1357, 1995.

34. Bleszynski, E., M. Bleszynski, and T. Jaroszewicz, "AIM: Adaptive integral method for solving large-scale electromagnetic scattering and radiation problems," *Radio Science*, Vol 31, No. 5, 1225–1251, Sep.–Oct. 1996.
35. Phillips, J. R. and J. K. White, "A precorrected-FFT method for electrostatic analysis of complicated 3-D structures," *IEEE Trans. Computer-Aided Design of Integrated Circuits and Systems*, Vol. 16, No. 10, 1059–1072, 1997.
36. Rokhlin, V., "Rapid solution of integral equations of scattering theory in two dimensions," *J. Comput. Physics*, Vol. 86, No. 2, 414–439, 1990.
37. Song, J. M. and W. C. Chew, "Multilevel fast-multipole algorithm for solving combined field integral equations of electromagnetic scattering," *Microw. Opt. Techn. Lett.*, Vol 10, No. 1, 14–19, 1995.
38. Song, J. M., C. C. Lu, and W. C. Chew, "Multilevel fast multipole algorithm for electromagnetic scattering by large complex objects," *IEEE Trans. Antennas Propag.*, Vol. 45, No. 10, 1488–1493, 1997.
39. Sheng, X.-Q., J.-M. Jin, J. Song, W. C. Chew, and C.-C. Lu, "Solution of combined-field integral equation using multilevel fast multipole algorithm for scattering by homogeneous bodies," *IEEE Trans. Antennas Propag.*, Vol. 46, No. 11, 1718–1726, 1998.
40. Pan, X.-M. and X.-Q. Sh, "A sophisticated parallel MLFMA for scattering by extremely large targets," *IEEE Antennas Propag. Mag.*, Vol. 50, No. 3, 129–138, 2008.
41. Ergül, Ö. and L. Gürel, "Rigorous solutions of electromagnetics problems involving hundreds of millions of unknowns," *IEEE Antennas Propag. Mag.*, Vol. 53, No. 1, 18–27, 2011.
42. Zhao, J.-S. and W. C. Chew, "Integral equation solution of Maxwell's equations from zero frequency to microwave frequencies," *IEEE Trans. Antennas Propag.*, Vol. 48, No. 10, 1635–1645, 2000.
43. Adams, R. J., "Physical and analytical properties of a stabilized electric field integral equation," *IEEE Trans. Antennas Propag.*, Vol. 52, No. 2, 362–372, 2004.
44. Vipiana, F., P. Pirinoli, and G. Vecchi, "A multiresolution method of moments for triangular meshes," *IEEE Trans. Antennas Propag.*, Vol. 53, No. 7, 2247–2258, 2005.
45. Andriulli, F. P., K. Cools, H. Bağci, F. Olyslager, A. Buffa, S. Christiansen, and E. Michielssen, "A multiplicative Calderon preconditioner for the electric field integral equation," *IEEE Trans. Antennas Propag.*, Vol. 56, No. 8, 2398–2412, 2008.
46. Qian, Z. G. and W. C. Chew, "An augmented electric field integral equation for high-speed interconnect analysis," *Microw. Opt. Techn. Lett.*, Vol. 50, No. 10, 2658–2662, 2008.
47. Andriulli, F. P., K. Cools, I. Bogaert, and E. Michielssen, "On a well-conditioned electric-field integral operator for multiple connected geometries," *IEEE Trans. Antennas Propag.*, Vol. 61, No. 4(2), 2077–2087, 2013.
48. Ylä-Oijala, P., M. Taskinen, and S. Järvenpää, "Surface integral equation formulations for solving electromagnetic scattering problems with iterative methods," *Radio Science*, Vol. 40, No. 6, RS6002, 2005.
49. Taskinen, M. and P. Ylä-Oijala, "Current and charge integral equation formulation," *IEEE Trans. Antennas Propag.*, Vol. 54, No. 1, 58–67, 2006.
50. Epstein, C. L. and L. Greengard, "Debye sources and the numerical solution of the time harmonic Maxwell equations," *Communications on Pure and Applied Mathematics*, Vol. LXIII, 413–463, 2010.
51. Markkanen, J., C.-C. Lu, X. Cao, and P. Ylä-Oijala, "Analysis of volume integral equations for scattering by high-contrast penetrable objects," *IEEE Trans. Antennas Propag.*, Vol. 60, No. 5, 2367–2374, 2012.
52. Ubeda, E. and J. M. Rius, "New electric-magnetic field integral equation for the scattering analysis of perfectly conducting sharp-edged objects at very low or extremely low frequencies," *2010 IEEE Antennas and Propagation Society International Symposium (APSURSI)*, Toronto, Canada, Jul. 11–17, 2010.

53. Ylä-Oijala, P., S. P. Kiminki, and S. Järvenpää, "Solving IBC-CFIE with dual basis functions," *IEEE Trans. Antennas Propag.*, Vol. 58, No. 12, 3997–4004, 2010.
54. Cools, K., F. P. Andriulli, D. De Zutter, and E. Michielssen, "Accurate and conforming mixed discretization of the MFIE," *IEEE Antennas Wirel. Propag. Lett.*, Vol. 10, 528–531, 2011.
55. Ubeda, E., J. M. Tamayo, and J. M. Rius, "Taylor-orthogonal basis functions for the discretization in method of moments of second kind integral equations in the scattering analysis of perfectly conducting or dielectric objects," *Progress In Electromagnetics Research*, Vol. 119, 85–105, 2011.
56. Ylä-Oijala, P., S. P. Kiminki, K. Cools, F. P. Andriulli, and S. Järvenpää, "Mixed discretization schemes for electromagnetic surface integral equations," *Internat. J. Num. Model.: Electronic Networks, Devices and Fields*, Vol. 25, No. 5, 525–540, 2012.
57. Markkanen, J., P. Ylä-Oijala, and A. Sihvola, "Discretization of the volume integral equation formulations for extremely anisotropic materials," *IEEE Trans. Antennas Propag.*, Vol. 60, No. 11, 5195–5202, 2012.
58. Yan, S. and J.-M. Jin, "Self-dual integral equations for electromagnetic scattering from IBC objects," *IEEE Trans. Antennas Propag.*, Vol. 61, No. 11, 5533–5546, 2013.
59. Dault, D. L., N. V. Nair, J. Li, and B. Shanker, "The generalized method of moments for electromagnetic boundary integral equations," *IEEE Trans. Antennas Propag.*, Vol. 62, No. 6, 3174-3188, 2014.
60. Ubeda, E., J. M. Rius, and A. Heldring, "Nonconforming discretization of the electric-field integral equation for closed perfectly conducting objects," *IEEE Trans. Antennas Propag.*, Vol. 62, No. 8, 4171–4186, 2014.
61. Ylä-Oijala, P., S. P. Kiminki, J. Markkanen, and S. Järvenpää, "Error-controllable and well-conditioned MoM solutions in computational electromagnetics: Ultimate surface integral equation formulation," *IEEE Antennas Propag. Magaz.*, Vol. 55, No. 6, 310-331, 2013.
62. Sihvola, A., *Electromagnetic Mixing Formulas and Applications*, IEE Electromagnetic Wave Series 47, IEE, Hertfordshire, United Kingdom, 1999.
63. Hoppe, D. J. and Y. Rahmat-Samii, *Impedance Boundary Conditions in Electromagnetics*, Taylor & Francis, Washington, DC, 1995.
64. Wallén, H., I. V. Lindell, and A. Sihvola, "Mixed-impedance boundary conditions," *IEEE Trans. Antennas and Propag.*, Vol. 59, No. 5, 1580–1586, 2011.
65. Lindell, I. V. and A. Sihvola, "Electromagnetic boundary conditions defined in terms of normal field components," *IEEE Trans. Antennas Propag.*, Vol. 58, No. 4, 1128–1135, 2010.
66. Lindell, I. V., *Methods for Electromagnetic Field Analysis*, 2nd edition, IEEE Press, New York, 1995.
67. Yaghijan, A. D., "Augmented electric- and magnetic-field integral equations," *Radio Science*, Vol. 16, No. 6, 987–1001, 1981.
68. Ylä-Oijala, P., M. Taskinen, and S. Järvenpää, "Analysis of surface integral equations in electromagnetic scattering and radiation problems," *Engineering Analysis with Boundary Elements*, Vol. 32, 196–209, 2008.
69. Ylä-Oijala, P. and M. Taskinen, "Application of combined field integral equation for electromagnetic scattering by dielectric and composite objects," *IEEE Trans. Antennas Propag.*, Vol. 53, No. 3, 1168–1173, 2005.
70. Harrington, R. F., "Boundary integral formulations for homogeneous material bodies," *Journal of Electromagnetic Waves and Applications*, Vol. 3, No. 1, 1–15, 1989.
71. Poggio, A. J. and E. K. Miller, "Integral equation solutions of three-dimensional scattering problems," *Computer Techniques for Electromagnetics*, R. Mittra (ed.), Pergamon Press, Oxford, U.K., 1973.
72. Medgyesi-Mitschang, L. N. and J. M. Putnam, "Integral equation formulations for imperfectly conducting scatterers," *IEEE Trans. Antennas Propag.*, Vol. 33, No. 2, 206–214, 1985.
73. Markkanen, J., P. Ylä-Oijala, and A. Sihvola, "Computation of scattering by DB objects with surface integral equation method," *IEEE Trans. Antennas Propag.*, Vol. 59, No. 1, 154–161, 2011.

74. Kiminki, S. P., J. Markkanen, and P. Ylä-Oijala, "Integral equation solution for the D'B' boundary condition," *IEEE Antennas Wirel. Propag. Lett.*, Vol. 9, 526–529, 2010.
75. Ylä-Oijala, P., M. Taskinen, and J. Sarvas, "Surface integral equation method for general composite metallic and dielectric structures with junctions," *Progress In Electromagnetic Research*, Vol. 52, 81–108, 2005.
76. Volakis, J. L., "Alternative field representations and integral equations for modeling inhomogeneous dielectrics," *IEEE Trans. Microw. Theory Techn.*, Vol. 40, 604–608, 1992.
77. Lu, C. C. and W. C. Chew, "A coupled surface-volume integral equation approach for the calculation of electromagnetic scattering from composite metallic and material targets," *IEEE Trans. Antennas Propag.*, Vol. 48, No. 12, 1866-1868, 2000.
78. Harrington, R. F., *Field Computation by Moment Methods*, Macmillan, New York, 1968.
79. Wilton, D. R., *Computational Methods, Chapter 1.5.5 in Scattering and Inverse Scattering in Pure and Applied Science*, Roy Pick and Pierre Sabatier (eds.), 316–365, Elsevier, 2002.
80. Hsiao, G. C. and R. E. Kleinman, "Mathematical foundations for error estimation in numerical solutions of integral equations in electromagnetics," *IEEE Trans. Antennas Propag.*, Vol. 45, No. 3, 316–328, 1997.
81. Bossavit, A., *Computational Electromagnetism, Variational Formulations, Complementary, Edge Elements*, Academic Press, San Diego, USA, 1998.
82. Monk, P., *Finite Element Methods for Maxwell's Equations*, Oxford Science Publications, Clarendon Press, Oxford, 2003.
83. Buffa, A., M. Costabel, and C. Schwab, "Boundary element methods for Maxwell's equations on non-smooth domains," *Numerische Mathematic*, Vol. 92, 679–710, 2002.
84. Warnick, K., *Numerical Analysis for Electromagnetic Integral Equations*, Artech House, 2008.
85. Wilton, D. R., S. M. Rao, A. W. Glisson, D. H. Schaubert, O. M. Al-Bundak, and C. M. Butler, "Potential integrals for uniform and linear source distributions on polygonal and polyhedral domains," *IEEE Trans. Antennas Propag.*, Vol. 32, No. 3, 276–281, 1984.
86. Graglia, R. D., "On the numerical integration of the linear shape functions times the 3-D Green's function or its gradient on a plane triangle," *IEEE Trans. Antennas Propag.*, Vol. 41, No. 9, 1448–1455, 1993.
87. Ylä-Oijala, P. and M. Taskinen, "Calculation of CFIE impedance matrix elements with RWG and nxRWG functions," *IEEE Trans. Antennas Propag.*, Vol. 51, No. 8, 1837–1846, 2003.
88. Järvenpää, S., M. Taskinen, and P. Ylä-Oijala, "Singularity subtraction technique for high-order polynomial vector basis functions on planar triangles," *IEEE Trans. Antennas Propag.*, Vol. 54, No. 1, 42–49, 2006.
89. Khayat, M. A. and D. R. Wilton, "Numerical evaluation of singular and near-singular potential integrals," *IEEE Trans. Antennas Propag.*, Vol. 53, No. 10, 3180–3190, 2005.
90. Polimeridis, A. G. and T. V. Yioultsis, "On the direct evaluation of weakly singular integrals in Galerkin mixed potential integral equation formulations," *IEEE Trans. Antennas Propag.*, Vol. 56, No. 9, 3011–3019, 2008.
91. Van Beurden, M. C. and S. J. L. van Eijndhoven, "Gaps in present discretization schemes for domain integral equations," *International Conference on Electromagnetics in Advanced Applications, ICEAA 2007*, Torino, 2007.
92. Van Beurden, M. C. and S. J. L. van Eijndhoven, "Well-posedness of domain integral equations for a dielectric object in homogeneous background," *J. Eng. Math.*, Vol. 62, 289–302, 2008.
93. Schaubert, D., D. Wilton, and A. Glisson, "A tetrahedral modeling method for electromagnetic scattering by arbitrarily inhomogeneous dielectric bodies," *IEEE Trans. Antennas Propag.*, Vol. 32, No. 1, 77–85, 1984.
94. Nedelec, J. C., "Mixed finite elements in R^3," *Numerische Mathematik*, Vol. 35, 315–341, 1980.
95. Christiansen, S. H. and J.-C. Nedelec, "A preconditioner for the electric field integral equation based on Calderon formulas," *SIAM J. Numerical Anal.*, Vol. 40, No. 3, 459–485, 2002.
96. Buffa, A. and S. H. Christiansen, "A dual finite element complex on the barycentric refinement,"

Math. Comput., Vol. 76, No. 260, 1743–1769, 2007.

97. Kiminki, S. P., I. Bogaert, and P. Ylä-Oijala, "Dual basis for the fully linear LL functions," *2012 IEEE International Symposium on Antennas and Propagation and USNC-URSI National Radio Science Meeting*, Chicago, Illinois, USA, Jul. 8–14, 2012.
98. Contopanagos, H., B. Dembart, M. Epton, J. J. Ottusch, V. Rokhlin, J. L. Fisher, and S. M. Wandzura, "Well-conditioned boundary integral equations for three-dimensional electromagnetic scattering," *IEEE Trans. Antennas Propag.*, Vol. 50, No. 12, 1824–1830, 2002.
99. Li, M and W. C. Chew, "Applying divergence-free condition solving the volume integral equations," *Progress In Electromagnetic Research*, Vol. 57, 311–333, 2006.
100. Markkanen J., P. Ylä-Oijala, and S. Järvenpää, "Volume integral equation formulations in computational electromagnetics," *International Conference on Electromagnetics in Advanced Applications*, Torino, Italy, Sep. 9–13, 2013.
101. Costabel, M., E. Darrigrand, and H. Sakly, "Essential spectrum of the volume integral operator in electromagnetic scattering by a homogeneous body," *Comptes Rendus Mathematique*, Vol. 350, No. 3–4, 193–197, 2012.
102. Hiptmair, R. and C. Schwab, "Natural boundary element methods for the electric field integral equation on polyhedra," *SIAM J. Numer. Anal.*, Vol. 40, No. 1, 66–86, 2002.
103. Buffa, A., R. Hiptmair, T. von Petersdorff, and C. Schawb, "Boundary element methods for Maxwell transmission problems in Lipschitz domains," *Numer. Math.*, Vol. 95, 459–485, 2003.
104. Müller, C., *Foundations of the Mathematical Theory of Electromagnetic Waves*, Springer, Berlin, 1969.
105. Liu, Y. A. and W. C. Chew, "Stability of surface integral equation for left-handed materials," *IET Microw. Antennas Propag.*, Vol. 1, No. 1, 84–89, 2007.
106. Ylä-Oijala, P. and M. Taskinen, "Improving conditioning of electromagnetic surface integral equations using normalized field quantities," *IEEE Trans. Antennas Propag.*, Vol. 55, No. 1, 178–185, 2007.
107. Wilton, D. R. and A. W. Glisson, "On improving stability of the electric field integral equation at low frequencies," *Proceedings of URSI Radio Science Meeting*, 24, Los Angeles, CA, Jun. 1981.
108. Mautz, J. R. and R. F. Harrington, "An E-field solution for a conducting surface small or comparable to the wavelength," *IEEE Trans. Antennas Propag.*, Vol. 32, No. 4, 330–339, 1984.
109. Wu, W.-L., A. W. Glisson, and D. Kajfez, "A study of two numerical solution procedures for the electric field integral equation at low frequency," *Appl. Comput. Soc. J.*, Vol. 10, No. 3, 69–80, 1995.
110. Ylä-Oijala, P. and M. Taskinen, "Well-conditioned Müller formulation for electromagnetic scattering by dielectric objects," *IEEE Trans. Antennas Propag.*, Vol. 53, No. 10, 3316–3323, 2005.
111. Vecchi, G., "Loop-star decomposition of basis functions in the discretization of the EFIE," *IEEE Trans. Antennas Propag.*, Vol. 47, No. 2, 339–346, 1999.
112. Andriulli, F. P., A. Tabacco, and G. Vecchi, "Solving the EFIE at low frequencies with a conditioning that grows only logarithmically with the number of unknowns," *IEEE Trans. Antennas Propag.*, Vol. 58, No. 5, 1614–1623, 2010.
113. Chen, S. Y., W. C. Chew, J. M. Song, and J.-S. Zhao, "Analysis of low-frequency scattering from penetrable scatterers," *IEEE Trans. Geosc. Remote Sensing*, Vol. 39, No. 4, 726–735, 2001.
114. Ylä-Oijala, P., S. P. Kiminki, and S. Järvenpää, "Electromagnetic surface integral equation representations in terms of scalar functions," *International Conference on Electromagnetics in Advanced Applications*, Torino, Italy, Sep. 9–13, 2013.
115. Gülzow, V., "An integral equation method for the time-harmonic Maxwell equations with boundary conditions for the normal components," *J. Integral Eq.*, Vol. 1, No. 3, 1988.
116. Stephanson, M. B. and J.-F. Lee, "Preconditioned electric field integral equation using Calderon identities and dual loop/star basis functions," *IEEE Trans. Antennas Propag.*, Vol. 57, No. 4, 1274–1279, 2009.

117. Bağci, H., F. P. Andriulli, K. Cools, F. Olyslager, and E. Michielssen, "A Caldern multiplicative preconditioner for the combined field integral equation," *IEEE Trans. Antennas Propag.*, Vol. 57, No. 10, 3387–3392, 2009.
118. Cools, K., F. P. Andriulli, and E. Michielssen, "A Calderon multiplicative preconditioner for the PMCHWT integral equation," *IEEE Trans. Antennas Propag.*, Vol. 59, No. 12, 4579–4587, 2011.
119. Begheim, Y., K. Cools, F. P. Andriulli, D. De Zutter, and E. Michielssen, "A Caldern multiplicative preconditioner for the PMCHWT equation for scattering by chiral objects," *IEEE Trans. Antennas Propag.*, Vol. 60, No. 9, 4239–4248, 2012.
120. Järvenpää, S. and P. Ylä-Oijala, "A global interpolator with low sample rate for multilevel fast multipole algorithm," *IEEE Trans. Antennas Propag.*, Vol. 61, No. 3, 1291–1300, 2013.
121. Gumerov, N. A. and R. Duraiswami, *Fast Multipole Methods for the Helmholtz Equation in Three Dimensions*, Elsevier, Amsterdam, The Netherlands, 2006.
122. Järvenpää, S., J. Markkanen, and P. Ylä-Oijala, "Broadband multilevel fast multipole algorithm for electric-magnetic current volume integral equation," *IEEE Trans. Antennas Propag.*, Vol. 61, No. 8, 4393–4397, 2013.
123. Jiang, L. J. and W. C. Chew, "Low-frequency fast inhomogeneous plane-wave algorithm (LF-FIPWA)," *Microw. Opt. Techn. Lett.*, Vol. 40, No. 2, 117–122, 2004.
124. Darve., E. and P. Have, "A fast multipole method for Maxwell's equations stable at all frequencies," *Phil. Trans. Royal Society of London A*, Vol. 362, No. 1816, 603–628, Mar. 2004.
125. Wallen, H. and J. Sarvas, "Translation procedures for broadband MLFMA," *Progress In Electromagnetic Research*, Vol. 55, 47–78, 2005.
126. Koc, S., J. Song, and W. C. Chew, "Error analysis for the numerical evaluation of the diagonal forms of the scalar spherical addition theorem," *SIAM J. Anal.*, Vol. 36, No. 3, 906–921, 1999.
127. Darve, E., "The fast multipole method: Numerical implementation," *J. Comput. Phys.*, Vol. 160, 195–240, 2000.
128. Sarvas, J., "Performing interpolation and anterpolation entirely by fast Fourier transform in the 3-D multilevel fast multipole algorithm," *SIAM J. Numer. Anal.*, Vol. 41, No. 6, 2180–2196, 2003.
129. Cecka, C. and E. Darve, "Fourier-based fast multipole method for the Helmholtz equation," *SIAM J. Sci. Comput.*, Vol. 35, No. 1, A79–A103, 2013.
130. Järvenpää, S. and P. Ylä-Oijala, "Multilevel fast multipole algorithm with local and global interpolators," *2013 IEEE International Symposium on Antennas and Propagation and USNCURSI National Radio Science Meeting*, Orlando, Florida, USA, Jul. 7–13, 2013.
131. Ergül, Ö. and L. Gŕel, "A hierarchical partitioning strategy for an efficient parallelization of the multilevel fast multipole algorithm," *IEEE Trans. Antennas Propag.*, Vol. 57, No. 6, 1740–1750, 2009.
132. Fostier, J. and F. Olyslager, "An asynchronous parallel MLFMA for scattering at multiple dielectric objects," *IEEE Trans. Antennas Propag.*, Vol. 56, No. 8, 2346–2355, 2008.
133. Li, M. K. and W. C. Chew, "Wave-field interaction with complex structures using equivalence principle algorithm," *IEEE Trans. Antennas Propag.*, Vol. 55, No. 1, 130–138, 2007.
134. Lancellotti, V., B. P. de Hon, and A. G. Tijhuis, "An eigencurrent approach to the analysis of electrically large 3-D structures using linear embedding via Green's operators," *IEEE Trans. Antennas Propag.*, Vol. 57, No. 11, 3575–3585, 2009.
135. Peng, Z., X.-C. Wang, and J.-F. Lee, "Integral equation based domain decomposition method for solving electromagnetic wave scattering from non-penetrable objects," *IEEE Trans. Antennas Propag.*, Vol. 59, No. 9, 3328–3338, 2011.
136. Georgieva, N. K., S. Glavic, M. H. Bakr, and J. W. Bandler, "Feasible adjoint sensitivity technique for EM design optimization," *IEEE Trans. Microw. Theory Techn.*, Vol. 50, No. 12, 2751–2758, 2002.
137. Nikolova, N. K., J. Zhu, D. Li, M. H. Bakr, and J. W. Bandler, "Sensitivity analysis of network parameters with electromagnetic frequency-domain simulators," *IEEE Trans. Microw. Theory Techn.*, Vol. 54, No. 2, 670–681, 2006.

138. Toivanen, J. I., R. A. E. Mäkinen, S. Järvenpää, P. Ylä-Oijala and J. Rahola, "Electromagnetic sensitivity analysis and shape optimization using method of moments and automatic differentiation," *IEEE Trans. Antennas Propag.*, Vol. 57, No. 1, 168–175, 2009.
139. Kataja, J. and J. I. Toivanen, "On shape differentiation of discretized electric field integral equation," *Eng. Anal. Boundary Elem.*, Vo. 37, No. 9, 1197–1203, 2013.
140. Kataja, J., S. Järvenpää, and R. A. E. Mäkinen, "Shape sensitivity analysis of electrically large metallic electromagnetic scatterers," *Opt-i, An International Conference on Engineering and Applied Sciences Optimization*, Kos Island, Greece, Jun. 4–6, 2014.